

A Periodic Table for Black Hole Orbits

Janna Levin^{*,†} and Gabe Perez-Giz^{**}

**Department of Physics and Astronomy,
Barnard College of Columbia University,
3009 Broadway, New York, NY 10027*

*†Institute for Strings, Cosmology and Astroparticle Physics,
Columbia University, New York, NY 10027 and*

***Physics Department, Columbia University, New York, NY 10027*

Understanding the dynamics around rotating black holes is imperative to the success of the future gravitational wave observatories. Although integrable in principle, test particle orbits in the Kerr spacetime can also be elaborate, and while they have been studied extensively, classifying their general properties has been a challenge. This is the first in a series of papers that adopts a dynamical systems approach to the study of Kerr orbits, beginning with equatorial orbits. We define a taxonomy of orbits that hinges on a correspondence between periodic orbits and rational numbers. The taxonomy defines the entire dynamics, including aperiodic motion, since every orbit is in or near the periodic set. A remarkable implication of this periodic orbit taxonomy is that the simple precessing ellipse familiar from planetary orbits is not allowed in the strong-field regime. Instead, eccentric orbits trace out precessions of multi-leaf clovers in the final stages of inspiral. Furthermore, for any black hole, there is some point in the strong-field regime past which zoom-whirl behavior becomes unavoidable. Finally, we sketch the potential application of the taxonomy to problems of astrophysical interest, in particular its utility for computationally intensive gravitational wave calculations.

I. INTRODUCTION

When Einstein realized his General Theory of Relativity correctly yielded the precession of the perihelion of Mercury, he had heart palpitations, later writing to Ehrenfest [1], “For some days I was beyond myself with excitement.” The anomalous precession of the perihelion of Mercury was the only astronomical observation in conflict with Newtonian gravity. Even taking account of perturbations from other planets, astronomers still saw Mercury’s perihelion overshoot its Keplerian target by an extra $43''$ /century, exactly the amount predicted by General Relativity.

Just shy of a century later, we are on the brink of another important test of General Relativity: the direct detection of gravitational waves. Black hole binaries may be the most viable candidates for a first direct detection. Consequently, and interestingly, the first gravitational waves observed will likely also probe relativistic orbits, which display exotic behaviors beyond even Mercury’s simple precessing ellipse. Relativistic orbital trajectories need not lie in a plane. They can also exhibit so-called “zoom-whirl” behavior – an extreme form of perihelion precession – whirling around the central black hole before zooming out quasi-elliptically [2, 3]. Nevertheless, even though orbits of a non-spinning test particle around a spinning black hole have been studied since Carter proved their integrability in the 1970’s [4], a language for making simple, general claims about their properties has been elusive.

In this paper, we introduce a powerful taxonomy that defines the full range of orbital dynamics in the equatorial plane of a Kerr black hole. We use this scheme to illustrate behaviors that run counter even to our relativistic intuitions. In the strong-field regime, precessing elliptical orbits such as Mercury’s are excluded. Instead, at close separations, eccentric orbits trace out precessions of patterns best described as multi-leaf clovers. We can also demarcate a region in orbital parameter space where the aforementioned zoom-whirl behavior is not merely prevalent but unavoidable, the size of that region increasing as the spin of the central black hole increases.

Not all orbits are created equal

Our taxonomy emphasizes a dynamically special set of orbits – the periodic orbits that return exactly to their initial conditions after a finite time. First widely touted by Poincaré [6], who suggested that the general behavior of any classical system could be gleaned from

a study of repeating motions, periodic orbits have played a crucial role in the treatment of some difficult problems in celestial mechanics, including the motions of planetary satellites, the long term stability of the solar system, and motion in galactic potentials. In contrast, periodic orbits in relativistic astrophysical systems like compact object binaries have gone largely unexamined¹, typically with the disclaimer that because they have measure zero in the space of all possible orbits, these closed orbits merit correspondingly little attention. Particularly in the case of test particle motion in the Schwarzschild and Kerr spacetimes – the only analytically soluble relativistic orbital systems – mapping out the properties of a particular measure zero set has seemed unnecessary.

By contrast, we will side with Poincaré. To paraphrase Orwell, while all measure zero sets are equal, some are more equal than others. For instance, circular orbits receive special attention, even though they are also a measure zero set, because they have two special dynamical features:

1. circular orbits are easy to handle, and
2. some orbits look like small perturbations to circular ones.

As a result, an analysis of circular orbits reveals fairly detailed information about nearby low-eccentricity orbits with relatively low overhead. Most relativity texts derive the famed precession of the perihelion of Mercury in precisely this way [14]. Of course, since most orbits are not close to circular ones, circular orbits alone do not encode the entirety of black hole orbital dynamics.

Remarkably, periodic orbits do. In fact they have even greater dynamical power than circular orbits because

1. periodic orbits are also easy to handle, and
2. *all* generic orbits look like small perturbations to periodic ones.

The latter fact, first noted by Poincaré, stems from a beautiful correspondence between periodic orbits and the rational numbers. The density of rationals on the number line thus implies a corresponding density of periodic orbits in the space of all possible orbits, so that

¹ While some authors [7, 8, 9, 10, 11, 12, 13] have explored inherently relativistic periodic motion, the systems studied have been more mathematically informative than astrophysically descriptive.

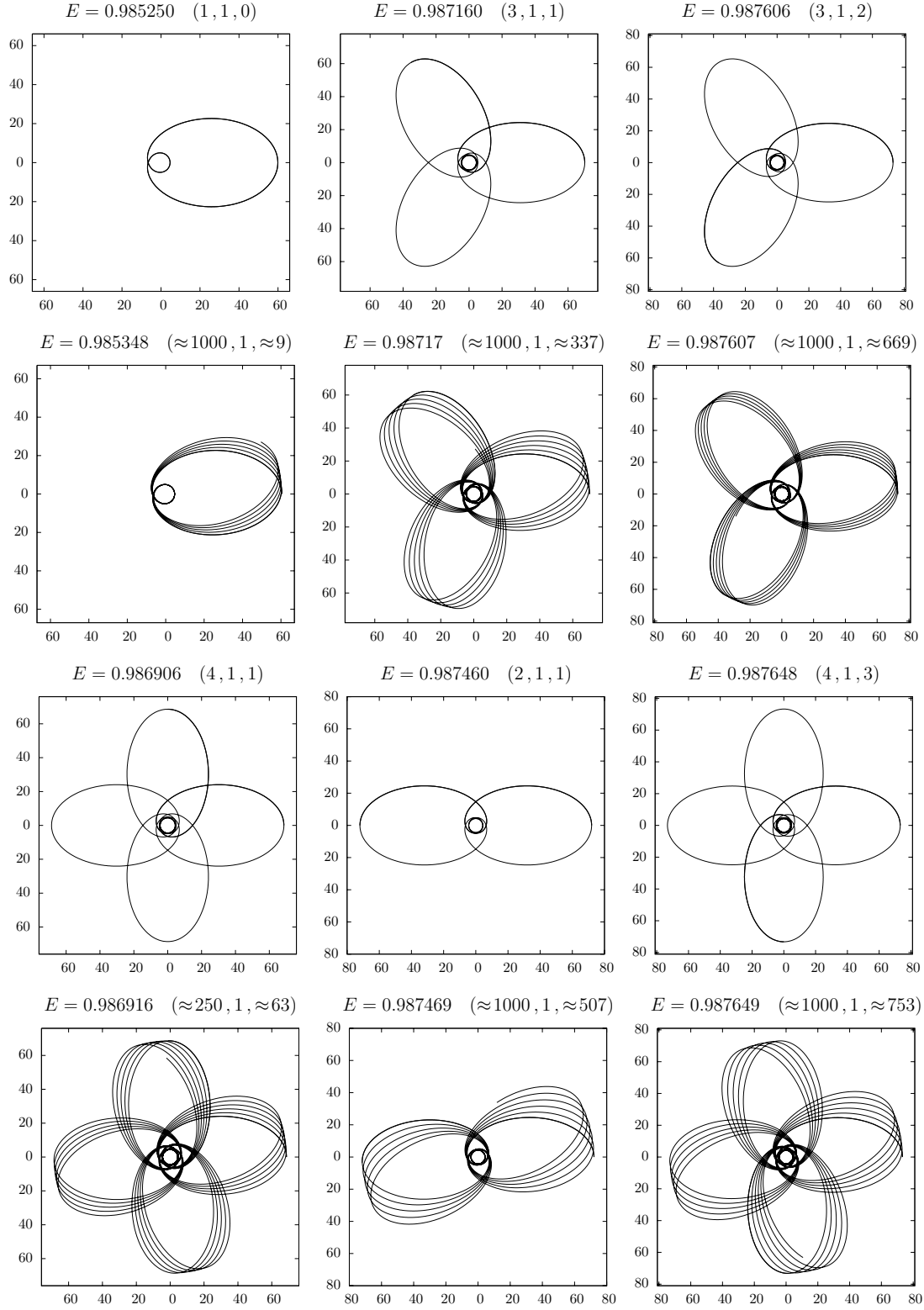


FIG. 1: This figure is a preview of figure 12. Rows 1 and 3 show exactly periodic orbits. Rows 2 and 4 show nearby aperiodic orbits.

any generic orbit can be viewed as an arbitrarily small deviation from some exactly periodic counterpart.

The result is a highly geometric skeleton of periodic orbits in terms of which the properties of even generic, aperiodic orbits can be described. Figure 1 offers a preview of the anatomy of this skeleton. Ignoring for the moment the details of these orbits, all of which are explained in the body of the paper, we can still see at a glance the two special dynamical properties discussed above. Rows 1 and 3 show a set of exactly periodic orbits. Besides being visually elegant, those correspond to a rational number according to a scheme detailed in §II. Just below each periodic orbit is a generic aperiodic orbit. Notice that each aperiodic orbit looks like a slow precession not of an ellipse but of the periodic orbit immediately above. Additionally, each such orbit can be assigned an approximating rational. What’s more, we can describe all black hole orbital dynamics by such a periodic table.

This paper is the first in a series that realizes Poincaré’s dictum for equatorial orbits in the Kerr spacetime². After defining and filling out this periodic skeleton for equatorial orbits (§II), we extract its dynamical consequences (§III), and explore its potential applications to a host of astrophysical problems (§IV). In particular, we outline how periodic orbits might facilitate the execution of the computationally intensive task of calculating the gravitational waveforms from extreme mass ratio inspirals [2, 3, 15, 16, 17, 18, 19].

Although important and interesting in its own right, for simplicity of presentation we relegate to an appendix the Hamiltonian formalism we use to identify periodic orbits in the Kerr system. For the body of the paper, the reader need only know that a is the spin parameter for each central black hole and that every orbit is specified by the energy E and angular momentum L of a test-particle as measured by an observer at infinity. As detailed in appendix A, we work in units in which a , E , L , and all coordinates and frequencies are dimensionless.

II. TAXONOMY OF PERIODIC ORBITS

The goal of this section is to detail a system for indexing all closed orbits around a black hole with a triplet of integers (z, w, v) . The reason behind the choice of symbols

² For clarity of exposition, we relegate the dynamically more involved nonequatorial Kerr orbits to another work.

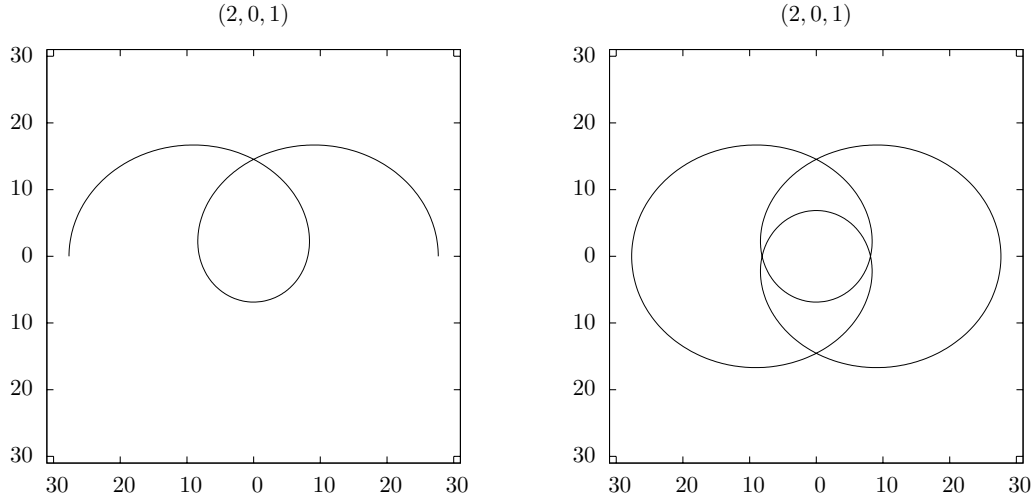


FIG. 2: Left: Half of the $(z = 2, w = 0, v = 1)$ periodic orbit. Right: The full $(z = 2, w = 0, v = 1)$ closed orbit. The orbit has $a = 0$, $L = 3.980393$, and $E = 0.973101$.

will become clear shortly. The scheme is topological, and our approach is to establish the connection between a given periodic orbit and its (z, w, v) label visually. We then establish the relationship between a given periodic orbit and a specific rational number in two ways: first based on topological features of the orbit, and then based on frequencies associated with its radial and azimuthal motions.

Finally, there is the matter of how we know that any particular periodic orbit we reference even exists. Answering this rather important question is the central objective of the dynamical section of the paper, §III.

A. The essential taxonomy

We have a simple topological method for identifying all of the closed orbits for a given angular momentum L around a given black hole (fixed by the spin a). Each periodic orbit traces out a finite number of leaves before closing. We will call the number of leaves z for zoom.³

Figure 2 shows a $z = 2$ orbit in the right panel, with a single radial cycle of the same orbit (from one apastron to periastron to the next apastron) shown in the left panel. Notice

³ Consider again the periodic orbits in rows 1 and 3 of figure 1. An immediately recognizable integer associated with each such orbit is the number of leaves it traces out before returning to its starting point. Each such leaf corresponds to the quasi-elliptical “zooming” behavior mentioned in the introduction.

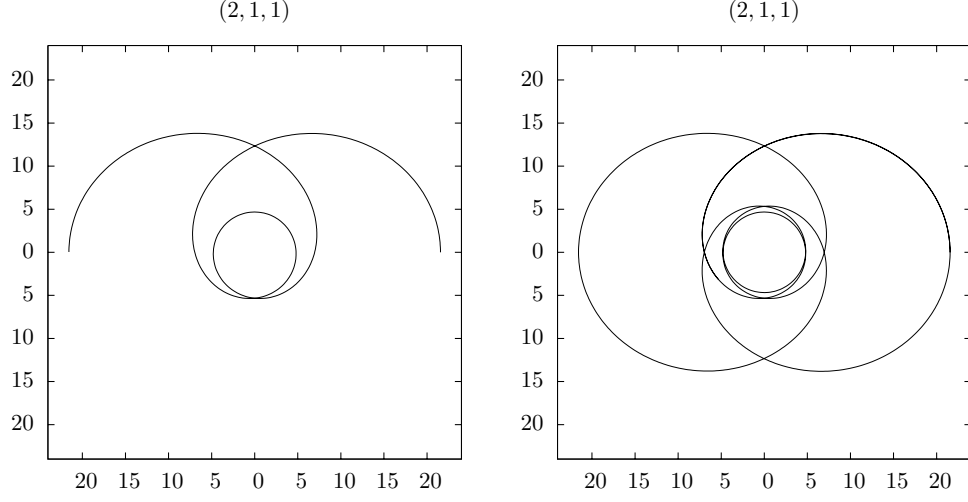


FIG. 3: Left: Half of the $(z = 2, w = 1, v = 1)$ periodic orbit. Right: The full $(z = 2, w = 1, v = 1)$ closed orbit. The orbital parameters are $a = 0$, $L = 3.718679$, and $E = 0.966555$.

from the figure that the accumulated angle from apastron to apastron, $\Delta\varphi_r$, is 3π . In a complete orbit, the accumulated angle is $\Delta\varphi = z\Delta\varphi_r = 6\pi$.

This is not, however, the only kind of $z = 2$ orbit. Figure 3 shows another 2-leaf orbit that whirls around the center an additional 2π before zooming out to apastron again. In fact, there is a 2-leaf orbit that whirls 4π longer around the center before returning to apastron, and in general one that whirls $2\pi w$ longer around the center before returning to apastron, for any positive integer w . Therefore, we will distinguish orbits by their number of whirls, w , as well as by z .

Still, z and w alone are not sufficient to specify the geometric features of a periodic orbit. To see this, note that the successive apastras of a periodic orbit with $z > 2$ form the vertices of a regular polygon. We will label the vertices of these polygons with a third integer v , counting the starting apastron of the orbit as $v = 0$ and increasing in the same rotational sense as the orbit (counterclockwise for prograde orbits, clockwise for retrograde orbits), as shown in figure 4. Now, given any $z > 2$, an orbit might move from the starting apastron immediately to the next vertex in the polygon. Such an orbit will be labelled $v = 1$. However, an orbit with the same (z, w) might skip the next neighbor vertex. We will assign that orbit a v of 2. In general, a periodic orbit with a given $z > 2$ can skip any number of vertices less than z when moving between successive apastras. All orbits will therefore be specified by (z, w, v) where v indicates the first vertex hit by the orbit after $v = 0$, and

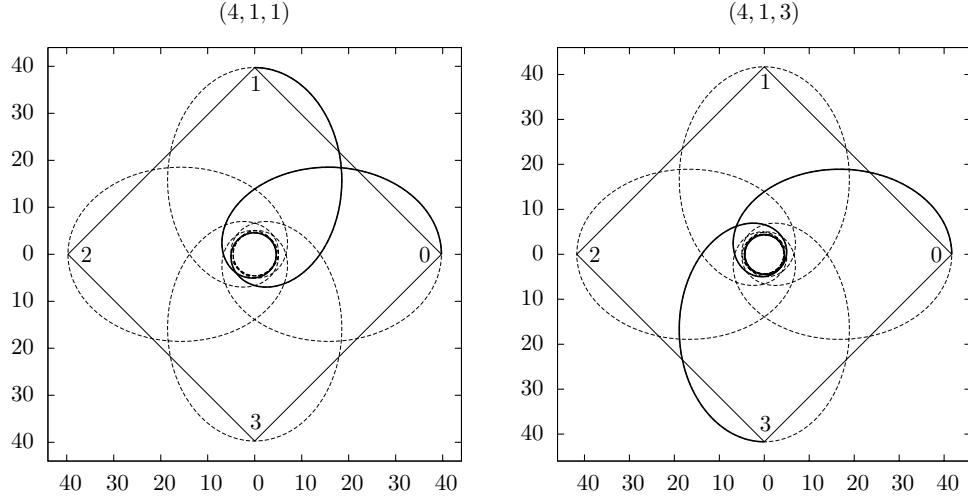


FIG. 4: 4-leafed orbits with no whirls. Left: Leaves are traced out in sequential order for the $(z = 4, w = 1, v = 1)$ closed orbit. Right: Leaves are traced out of order for the $(z = 4, w = 1, v = 3)$ closed orbit. The orbital parameters are $a = 0, L = 3.834058$ for both. The energy of the leftmost orbit is $E = 0.979032$ and the energy of the rightmost orbit is $E = 0.979842$.

where v has the range

$$1 \leq v \leq z - 1 \quad . \quad (1)$$

The orbit on the left of figure 4 for instance is a $(4, 1, 1)$ while the orbit drawn on the right is a $(4, 1, 3)$. We can still use eqn. (1) for the $z = 2$ leaf orbits, despite the fact that two points do not trace out a polygon, so that $v = 1$. Following this rubric, the orbit of figure 2 is a $(2, 0, 1)$ and that of figure 3 is a $(2, 1, 1)$.

Single leaf orbits, such as those shown in figure 5, need separate discussion. Instinctively, we want to assign them a z value of 1, but then the v restricted by the range in (1) would be undefined. We can handle this problem by assigning such orbits $v = 0$, since successive apastras for these orbits are actually the same single apastron. That would lead us to modify the allowed range of v to

$$\begin{aligned} 1 \leq v \leq z - 1 \quad , \quad \text{if } z > 1 \\ v = 0 \quad , \quad \text{if } z = 1 \quad . \end{aligned} \quad (2)$$

There is another degeneracy to address. For a given w , some (z, v) pairs describe the same orbit. For instance, the $(4, 1, 2)$ orbit closes after only two leaves and is identical with the $(2, 1, 1)$ with the same orbital parameters. We remove this degeneracy by requiring that

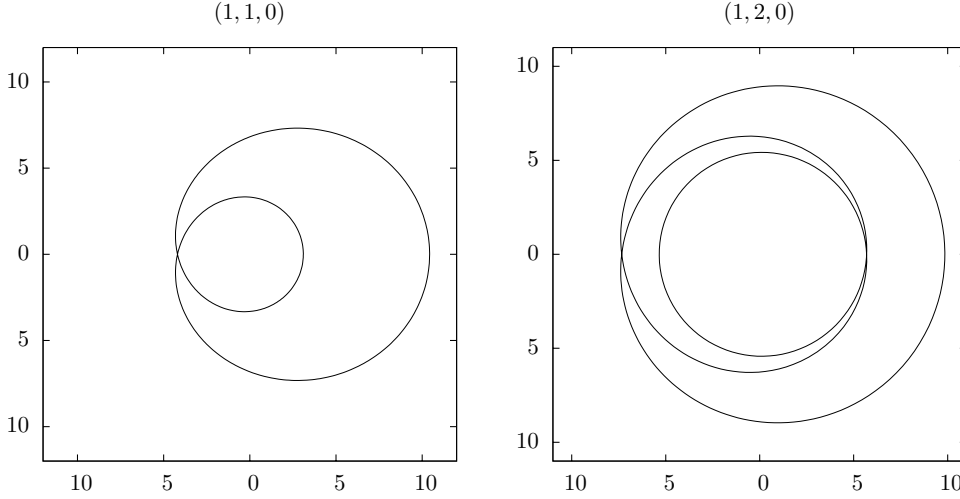


FIG. 5: Left: The full $(z = 1, w = 1, v = 0)$ closed orbit. The orbital parameters are $a = 0$, $L = 2.714326$, and $E = 0.932703$. Right: The full $(z = 1, w = 2, v = 0)$ closed orbit. The orbital parameters are $a = 0$, $L = 3.535534$, and $E = 0.948491$.

z and v be relatively prime. The allowed v are then

$$\begin{aligned} 1 \leq v \leq z - 1 \quad , \quad & \text{if } z > 1, z \bmod v = 0 \\ v = 0 \quad , \quad & \text{if } z = 1 \quad . \end{aligned} \quad (3)$$

Having pruned those orbits out of any counting, the (z, w, v) label now uniquely specifies the topological features of a closed orbit.

B. Periodic orbits and rational numbers

Our (z, w, v) taxonomy naturally forges the relationship between rational numbers and periodic orbits. Note first that any positive rational number q can be written in the form

$$q = s + \frac{m}{n} \quad , \quad (4)$$

where $s \geq 0$ is the integer part and m/n is the fractional part, with m and n relatively prime integers satisfying

$$1 \leq m \leq n - 1 \quad . \quad (5)$$

Of course, these are exactly the conditions that w, v and z satisfy. Since every periodic orbit corresponds to a (z, w, v) set in our scheme, we can therefore associate a rational number

$$q \equiv w + \frac{v}{z} \quad (6)$$

to every periodic orbit. This association reflects the physical observation that for a periodic orbit, the accumulated azimuth between successive apastra must be given by

$$\Delta\varphi_r = 2\pi \left(1 + w + \frac{v}{z}\right) = \frac{\Delta\varphi}{z} \quad , \quad (7)$$

where the total accumulated angle $\Delta\varphi$ in one full orbital period is $z\Delta\varphi_r$.

There is another sense in which we can associate a rational number to a periodic orbit. Every eccentric equatorial orbit has 2 associated orbital frequencies: a radial frequency

$$\omega_r = \frac{2\pi}{T_r} \quad , \quad (8)$$

where T_r is the (coordinate) time elapsed during one radial cycle (not the total period of an orbit), and an angular frequency

$$\omega_\varphi = \frac{1}{T_r} \int_0^{T_r} \frac{d\varphi}{dt} dt = \frac{\Delta\varphi_r}{T_r} \quad (9)$$

corresponding to the time-averaged value of $d\varphi/dt$ over one radial period. For a generic orbit, the ratio of those frequencies can be arbitrary, but for a periodic orbit, it must satisfy

$$\frac{\omega_\varphi}{\omega_r} = \frac{\Delta\varphi_r}{2\pi} = 1 + w + \frac{v}{z} = 1 + q \quad . \quad (10)$$

The periodic orbits, then, are those whose fundamental orbital frequencies are rationally related.

It is worth noting that the orbital frequencies ω_r and ω_φ are the same frequencies that arise in an action-angle Hamiltonian formulation of the dynamics [23]. We draw the connection explicitly in appendix B.

C. Circular orbits

Circular orbits, while strictly periodic, do not fit into our indexing scheme. This is not surprising, since circular orbits close compulsorily rather than by the tuning of any orbital parameters. Put in other terms, a circular orbit has only a single rotational frequency ω_φ ; there is no additional librational frequency to which it must relate rationally in order to close. Circular orbits exhibit a periodicity of a different flavor, and no association to rational numbers is required. They are, in a sense, periodic by default.

Perhaps unexpectedly, there is nonetheless a natural way to fit the *stable* circular orbits into our taxonomy. Consider, for a given black hole spin a , all the orbits with a given angular

momentum L . For such a fixed a, L pair, the frequencies ω_φ and ω_r vary continuously⁴ with eccentricity. Not surprisingly, the zero eccentricity limit of ω_φ is just the $d\varphi/dt$ of the stable circular orbit. Additionally, as detailed in appendix C, the zero eccentricity limit of ω_r is not zero but rather the frequency of radial oscillations for small perturbations of the circular orbit. In this limiting sense, then, we can assign every stable circular orbit an effective

$$q_c = \lim_{e \rightarrow 0} \left(\frac{\omega_\varphi}{\omega_r} - 1 \right) \quad (11)$$

and thus an effective (z, w, v) triplet.

As shown in Appendix C, q_c grows monotonically with decreasing r_c , the radius of the stable circular orbit. In fact, it turns out that for a given a , every positive rational q corresponds to some stable circular orbit, with $q_c \rightarrow 0$ as the circular radius $r_c \rightarrow \infty$ and $q_c \rightarrow \infty$ as $r_c \rightarrow r_{ISCO}$, the radius of the innermost stable circular orbit. At low r , q_c will eventually go above 1 so that $w_c > 1$. Additionally, the corresponding z_c will sometimes be small ($z \lesssim 10$). Both these facts will leave their footprint on orbits in the strong-field regime.

D. Precession of periodic orbits

Our taxonomy focuses on the set of measure zero closed orbits. A generic orbit will experience an accumulated angle that is irrational so the orbit precesses and never closes. However, since the rationals are dense on the number line, any generic orbit can be approximated arbitrarily closely by some rational. Therefore, although it seems that we are describing a special set of extremely rare orbits, we might as well be describing every orbit. The potential power of this taxonomy lies in this simple observation.

To illustrate the approximation of a generic orbit by periodic ones, consider the $(3, 1, 1)$ closed multi-leaf orbit on the left of figure 6. There are aperiodic orbits which lie close to this orbit. For instance consider an orbit that accumulates a slightly greater angle in one cycle from apastron to apastron, $w + v/z = 1 + 1/3 + \delta$ where the irrational $\delta \ll 1$. It's three leaf pattern will precess, never closing. The precessing orbit could be approximated by the periodic orbit $(3, 1, 1)$. The smaller the precession, the better the approximation. Or,

⁴ In fact, as we'll see in Sections III A and III B, they vary monotonically with energy and eccentricity at fixed a, L .

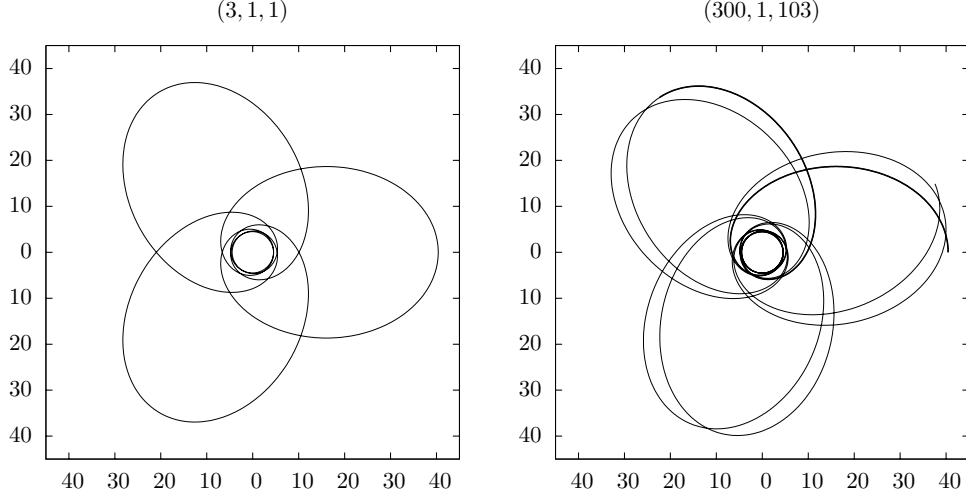


FIG. 6: Left: The closed $(z = 3, w = 1, v = 1)$ orbit. right: The closed $(z = 300, w = 1, v = 103)$ orbit looks like a precession of the $(z = 3, w = 1, v = 1)$ orbit. Only 6 of the 300 leaves are shown. The first segment from apastron to apastron is emphasized in bold. The orbital parameters are $a = 0, L = 3.834058$ for both. The leftmost orbit has energy $E = 0.979304$ and the rightmost orbit has energy $E = 0.979331$.

we could do better. For the sake of argument, let's approximate the irrational drift by the rational $\delta \approx 1/100$ and write $w + v/z = 1 + 1/3 + 1/100$ as $w + v/z = 1 + 103/300$. We can now approximate the precessing orbit by the $(300, 1, 103)$ multi-leafed orbit on the right of figure 6. Our rational approximate is a 300-leaf orbit. Since $v = 103$, it skips 102 leaves in the pattern each time it moves out to apastron so that it appears to trace out a precessing three leaf pattern. The periodic approximate does actually close but only after tracing all 300 leaves.

We emphasize that the approximation of generic orbits by a nearby periodic is a reality foisted on us by finite precision, both numerically and observationally. Every computer program truncates numbers to some finite precision and in so doing explicitly outputs a rational. Every measurement performed delivers an observable to some finite precision and in so doing explicitly delivers all data as rationals. Likewise, every calculated aperiodic black hole orbit will necessarily be indistinguishable from some periodic one. We have no choice about this. The taxonomy embraces that fact and allows us to estimate the rational approximate deliberately rather than inadvertently through the restrictions of finite precision.

E. Not all orbits allowed

An obvious question to ask is whether all periodic orbits are allowed in every Kerr system. In other words, is every rational in the set $0 < q < \infty$ allowed? The answer will turn out to be a very interesting no.

III. BLACK HOLE ORBITAL DYNAMICS

Indeed, not all periodic orbits are allowed in a given Kerr system. We now show that the rational numbers occur in the range

$$q_c \leq q \leq q_{max} \quad , \quad (12)$$

bounded below by the q_c of the stable circular orbit and above by the q_{max} of the maximum energy bound orbit.⁵ Periodic orbits corresponding to all rational numbers in this range populate the phase space. The limits vary not only for different black hole spins, but also for different values of the constant angular momentum L , as we will demonstrate in §III A and §III B.

Equation (12) turns out to be profound. The crucial insight that allows us to determine the admissible periodic orbits is the observation that $\Delta\varphi_r$, and therefore the associated rational $q = w + v/z$, increase monotonically with energy. We extract the dynamical consequences of this fact, contrasting the weak and strong-field behaviors.

A. The Schwarzschild zoo

To appreciate the significance of observation (12), we first consider Schwarzschild ($a = 0$) orbits because they admit a formal effective potential formulation that lends clarity to the discussion. Schwarzschild orbits can be described as one-dimensional motion in an effective potential [14]:

$$\frac{1}{2}\dot{r}^2 + V_{\text{eff}} = \varepsilon_{\text{eff}} \quad (13)$$

where

$$\varepsilon_{\text{eff}} = \frac{1}{2}E, \quad V_{\text{eff}} = \frac{1}{2} - \frac{1}{r} + \frac{L^2}{2r^2} - \frac{L^2}{r^3} \quad . \quad (14)$$

⁵ To be definite, we mean *non-plunging*, bound orbit.

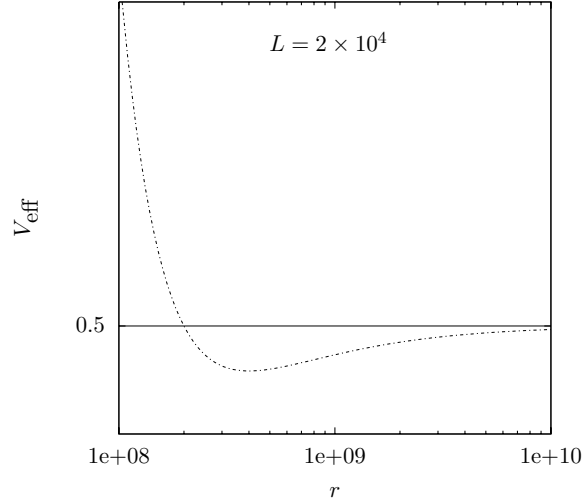


FIG. 7: The effective radial potential $V_{\text{eff}}(r)$ for very large r (plotted on a $\ln r$ scale) in the vicinity of solar system values. The horizontal line at $V_{\text{eff}} = 1/2$ corresponds to particle energy $E = 1$.

Since the shape of the potential is fixed by the value of L , a given V_{eff} snapshot is tantamount to a snapshot of the family of orbits with the same angular momentum. Consider the effective potentials of figures 7, 8(a), and 9(a), which show V_{eff} 's ranging from large L to low L , or equivalently successive V_{eff} 's from the weak-field to the strong-field regimes. Clearly, the stable circular orbit always has the lowest energy for a given L . If, as we will show, $\Delta\varphi_r = 2\pi(q + 1)$ increases monotonically with energy, it must also be the case that $q = w + v/z$ increases monotonically. It follows immediately that eqn. (12) is true. We verify these claims for the Schwarzschild spacetime in this section.

Spinning black hole spacetimes do not admit a comparable one-dimensional effective potential description. However, all the qualitative features of the Schwarzschild analysis survive and, in fact, all the interesting dynamical effects become more pronounced. We outline the dynamical results for the spinning black hole spacetime in §III B.

We begin in the weak-field regime at large radii (large L) and will watch the dynamics evolve as we move into the strong-field regime at close separations (low L). Consider, for instance, solar system values, so that L is in the range of Mercury's angular momentum $L \sim 2 \times 10^4$. Such a potential at large r is shown in figure 7. There is effectively a large centrifugal barrier at low r . The energy of the bound orbits ranges from $E = 1$ for the eccentricity $e = 1$ trajectory down to the stable circular orbit $e = 0$. (Following the

standard convention in the literature we define eccentricity as

$$e = \frac{r_a - r_p}{r_a + r_p} \quad , \quad (15)$$

where r_a is the apastron and r_p is the perihelion.)

All of the bound orbits with this L are well described as minute precessions of an ellipse. In our taxonomy, these orbits correspond to $(z, 0, 1)$ with a very high number of zooms z ($q = w + v/z \ll 1$). Mercury, for instance, precesses roughly $43''/\text{century}$. With an orbital period of 88 days, this comes to roughly $0.1''/\text{orbit}$, which is $\sim 360^\circ/(3600^2)$. Mercury, therefore, is close to a periodic orbit with $z = 3600^2 = 1.296 \times 10^7$ leaves and no whirls, which always advances to the next available apastron – that is, a $(1.296 \times 10^7, 0, 1)$. Even the perfectly periodic $(1.296 \times 10^7, 0, 1)$ will give the appearance of a simple precessing ellipse.

In figure 8, we move into the intermediate-field regime and show the potentials for angular momenta $L = 4.1$ and $L = 4.5$, with the centrifugal barrier better resolved to show the unstable $E > 1$ circular orbit.

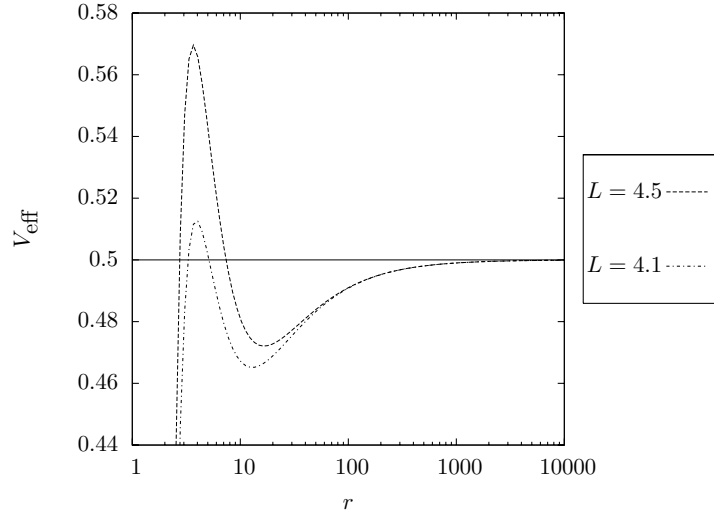
The key conclusions for the black hole dynamics comes from the simple figures 8(b) and 8(c). Some salient features turn out to be universal for all L . Most important, figures 8(b) and 8(c) show that, for a fixed L , $q = w + v/z$ increases monotonically with both E and e and terminates at some finite value. As per the comments at the beginning of §III, this justifies eqn. (12).

There are other interesting dynamical features evident from these figures alone. For instance, we see that no orbits in this intermediate L range whirl since $q = w + v/z < 1$ and therefore $w = 0$ over the entire range of eccentricities. Incidentally, the same thing is true for the planetary L (whose q versus e plot we omitted because it was graphically indistinguishable from the $q = 0$ axis). This explains why we do not see zoom-whirl behavior in the solar system, or for that matter, even for Schwarzschild orbits whose periastra are as close to the black hole as $r \approx 8$.

For $L = 4.5$, the allowed closed orbits correspond to rational numbers bounded by the range

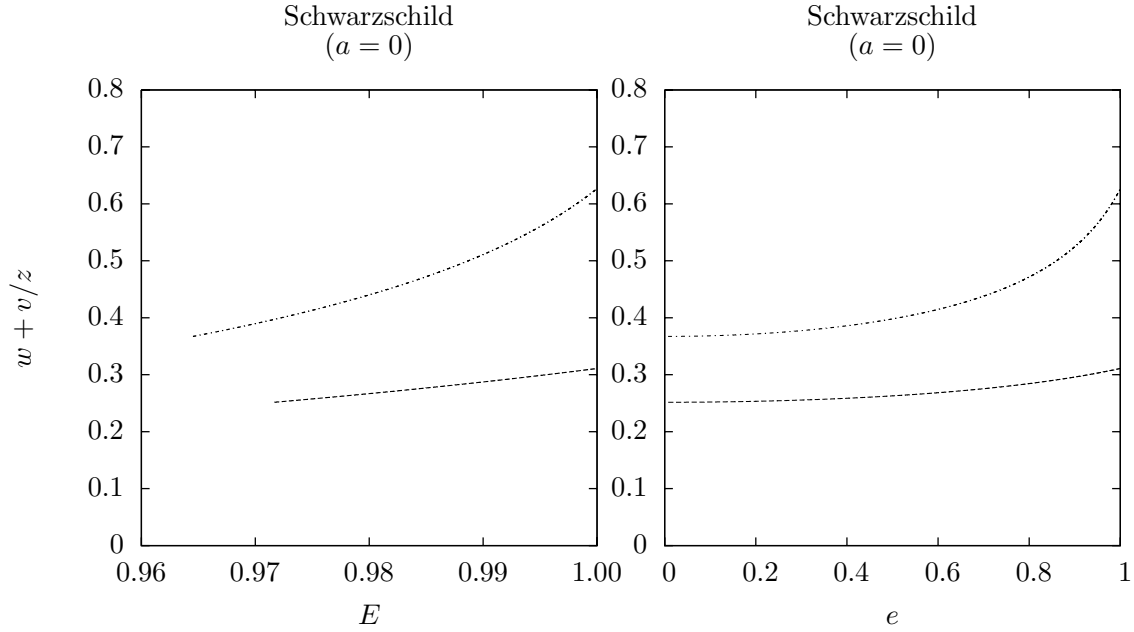
$$\frac{1}{4} \lesssim q \lesssim \frac{3}{10} \quad , \quad (16)$$

where we have approximated the limits by the nearest low v, z option ($w = 0$). It follows that all orbits for $L = 4.5$ will look like precessions of $(4, 0, 1)$ not quite going over to precessions of $(3, 0, 1)$ at the upper limit as they march through the rationals with energy increasing to



(a) The effective radial potential $V_{\text{eff}}(r)$ as a function of r on a log scale for L just above L_{IBCO} . The horizontal line at $V_{\text{eff}} = 1/2$ corresponds to particle energy $E = 1$. The y -axis ranges from

$$0.5 + 9 \times 10^{-9} \text{ down to } 0.5 - 3 \times 10^{-9}.$$



(b) $w + v/z$ versus energy.

(c) $w + v/z$ versus eccentricity.

FIG. 8: Schwarzschild, values of L just above L_{IBCO} . In terms of accumulated angle, $(\Delta\varphi_r/2\pi) - 1 = w + v/z$.

$E = 1$. This is dramatically different from Mercury-type motion. These are not precessing ellipses but are precessions of a four-leaf clover.

As the angular momentum drops even further to $L = 4.1$, the allowed closed orbits correspond to rational numbers bounded by the range

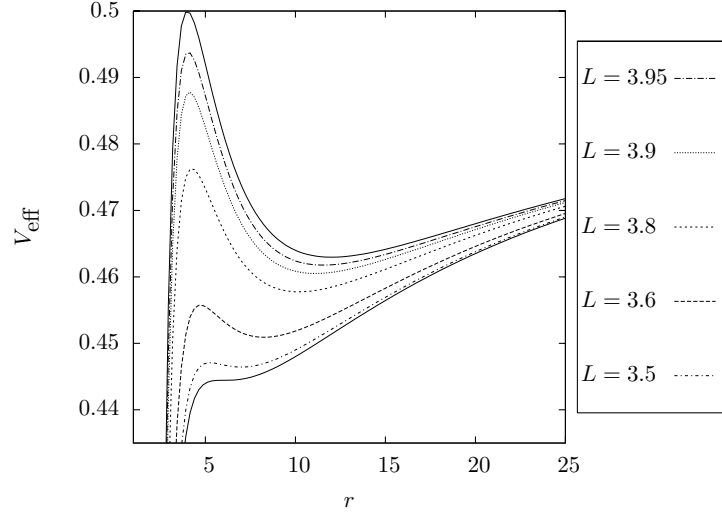
$$\frac{3}{8} \lesssim q \lesssim \frac{3}{5} \quad , \quad (17)$$

where we have approximated the limits by the nearest low v, z option. Orbits will pass through $3/8, 2/5, 3/7, 1/2, 4/7$, to $3/5$ and all the rationals in between as the energy increases from that of the stable circular to $E = 1$.

The zoo becomes more crowded as the angular momentum drops to the point that the energy of the unstable circular orbit drops below 1. The top darkened curve in figure 9(a) is the potential for $L = L_{IBCO} = 4$, the angular momentum of the innermost bound circular orbit (IBCO). The bottom darkened curve is the potential for $L = L_{ISCO} = \sqrt{12}$, the angular momentum of the innermost stable circular orbit (ISCO). For every $L_{ISCO} < L < L_{IBCO}$, several of which figure 9(a) shows, there is an energetically bound ($E < 1$) unstable circular orbit. Accompanying each bound unstable circular orbit is an eccentric orbit called a homoclinic orbit. These orbits are so central to the discussion of strong-field dynamics that we now briefly outline how they fit into the (z, w, v) taxonomy before continuing with the rest of the dynamical discussion.

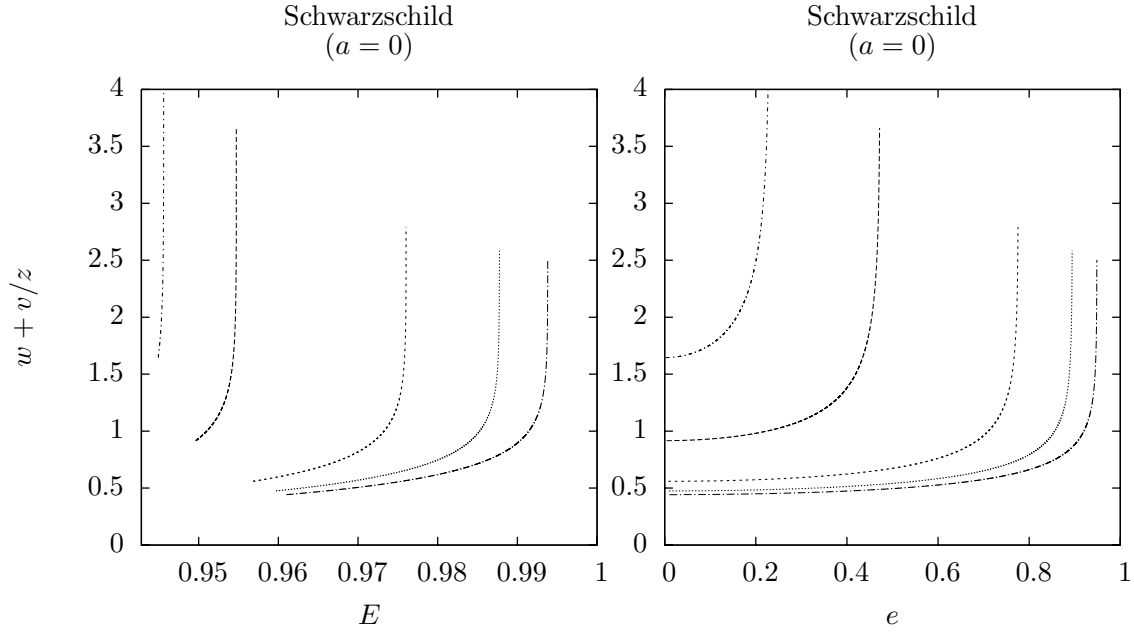
A homoclinic orbit asymptotically recedes from a periodic orbit (in this case, an unstable circular orbit) in the infinite past, zooms out to some finite apastron, and then asymptotically approaches the same periodic orbit in the infinite future. Though eccentric, each homoclinic orbit has the same energy E_u and angular momentum L_u as the unstable circular orbit to which it asymptotes. When it exists, a homoclinic orbit forms the boundary (for a given L) between orbits that plunge over the top of the potential ($E > E_u$) and orbits that do not ($E < E_u$).

To see the role of homoclinic orbits in our taxonomy, consider the behavior of a homoclinic orbit that starts at apastron, such as the one in figure 10. As the particle climbs toward the maximum of the effective potential, it asymptotes toward the circular orbit located there and executes an infinite number of whirls. Because it never returns to apastron, the homoclinic orbit is not strictly periodic. Nevertheless, it is appropriate to think of this single leaf orbit as the $w \rightarrow \infty$ limit of the progression of the $(1, w, 0)$ orbits. We thus label each homoclinic



(a) The effective radial potential $V_{\text{eff}}(r)$ bounded on the top by

$$L_{IBCO} = 4 \text{ and on the bottom by } L_{ISCO} = \sqrt{12}.$$



(b) $w + v/z$ versus energy.

(c) $w + v/z$ versus eccentricity.

FIG. 9: Schwarzschild for $L_{ISCO} < L < L_{IBCO}$. In terms of accumulated angle, $(\Delta\varphi_r/2\pi) - 1 = w + v/z$.

orbit as $(1, \infty, 0)$, so that each has an associated rational $q = \infty$.

It is perhaps surprising that the $q = \infty$ orbits are bound and have eccentricities $e < 1$. More specifically, homoclinic orbits with $L \rightarrow L_{IBCO}$ have eccentricities $e \rightarrow 1$, while those

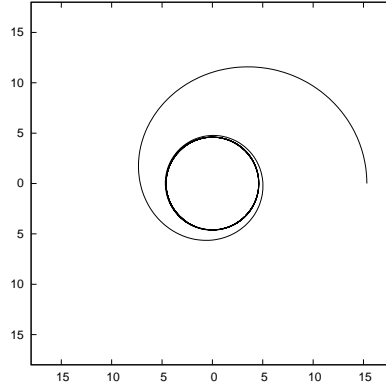


FIG. 10: A homoclinic orbit $(1, \infty, 0)$ for $L_{ISCO} < L < L_{IBCO}$. The orbital parameters are $a = 0, L = 3.636619$, and $E = 0.958373$.

with $L \rightarrow L_{ISCO}$ have $e \rightarrow 0$. In fact, the ISCO *is* just the zero eccentricity homoclinic orbit. Properties of homoclinic orbits beyond what is needed for the current discussion, including analytic expressions for their trajectories, can be found in Refs. [13, 21].

Since the homoclinic orbit is the maximum energy bound orbit (for a given L , it defines the upper range of allowed periodic orbits, a la eqn. (12). Therefore $q_{max} = \infty$ for all $L_{ISCO} < L < L_{IBCO}$. As always, the lower bound is greater than zero because q terminates at a finite value.

To see the consequences of this fact, consider the $L = 3.9$ line in figure 9(b), which shows a q_c of approximately $0.475 \approx 19/40$. By eqn. (12), we have the bound

$$\frac{19}{40} \leq q \leq \infty \quad (18)$$

for $L = 3.9$. We can approximate the lower limit better by going to higher v, z , but these values are sufficient to make a point: there are no Mercury type motions. Rather, small perturbations of the circular orbit can be approximated by a periodic orbit with 40 leaves that jumps 19 apastras away every radial cycle. Such an orbit will look very much like a precession of a two-leaf orbit. Again, the one-leaf, zero-whirl orbit is forbidden. The $(1, 0, 0)$ corresponds to a $q = 0$ and is not reached by any $L = 3.9$ orbit as figure 9(b) shows.

Finally, figure 11 shows a periodic table of orbits (still for $L = 3.9$). For illustration, we only include orbits with z up to 3, although the spectrum allows $z \rightarrow \infty$ orbits. The first column corresponds to $w = 0$, the middle column to $w = 1$ and the last column to $w = 2$. The series could be continued through to $w \rightarrow \infty$. The sequence should be read from top to bottom and then from left to right to indicate increasing energy. Notice that the first

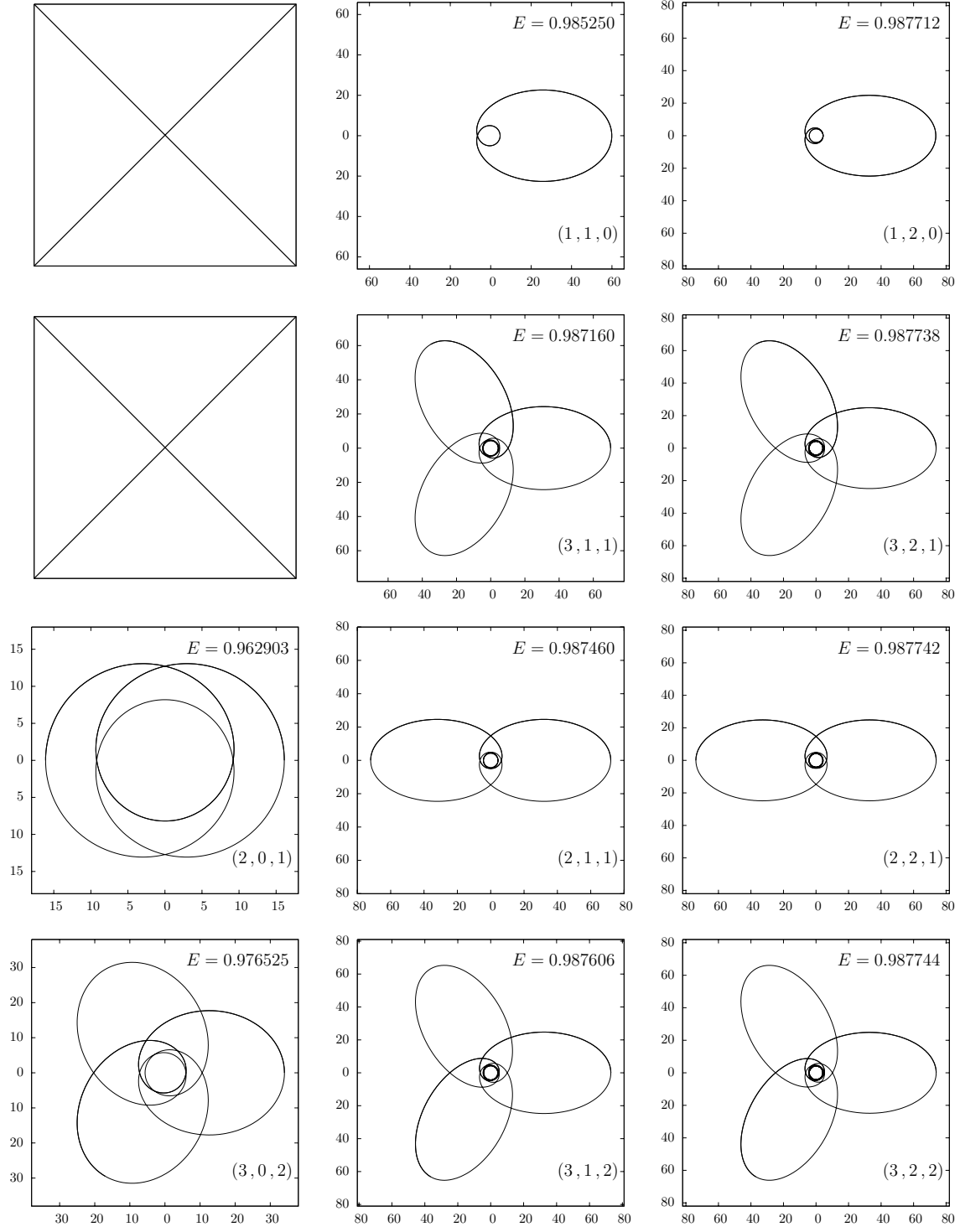


FIG. 11: All $z = 1, 2, 3$ orbits with $w = 0$ for the first column, $w = 1$ for the middle column, and $w = 2$ for the last column. All orbits lie on the $L = 3.9$ line of figure 9. Norbits increase in energy from top to bottom and left to right. The first radial cycle is emphasized in bold for each orbit. Notice the first and second entry in the first column are blank, indicating the inaccessibility of the $(1, 0, 0)$ and $(3, 0, 1)$ orbits.

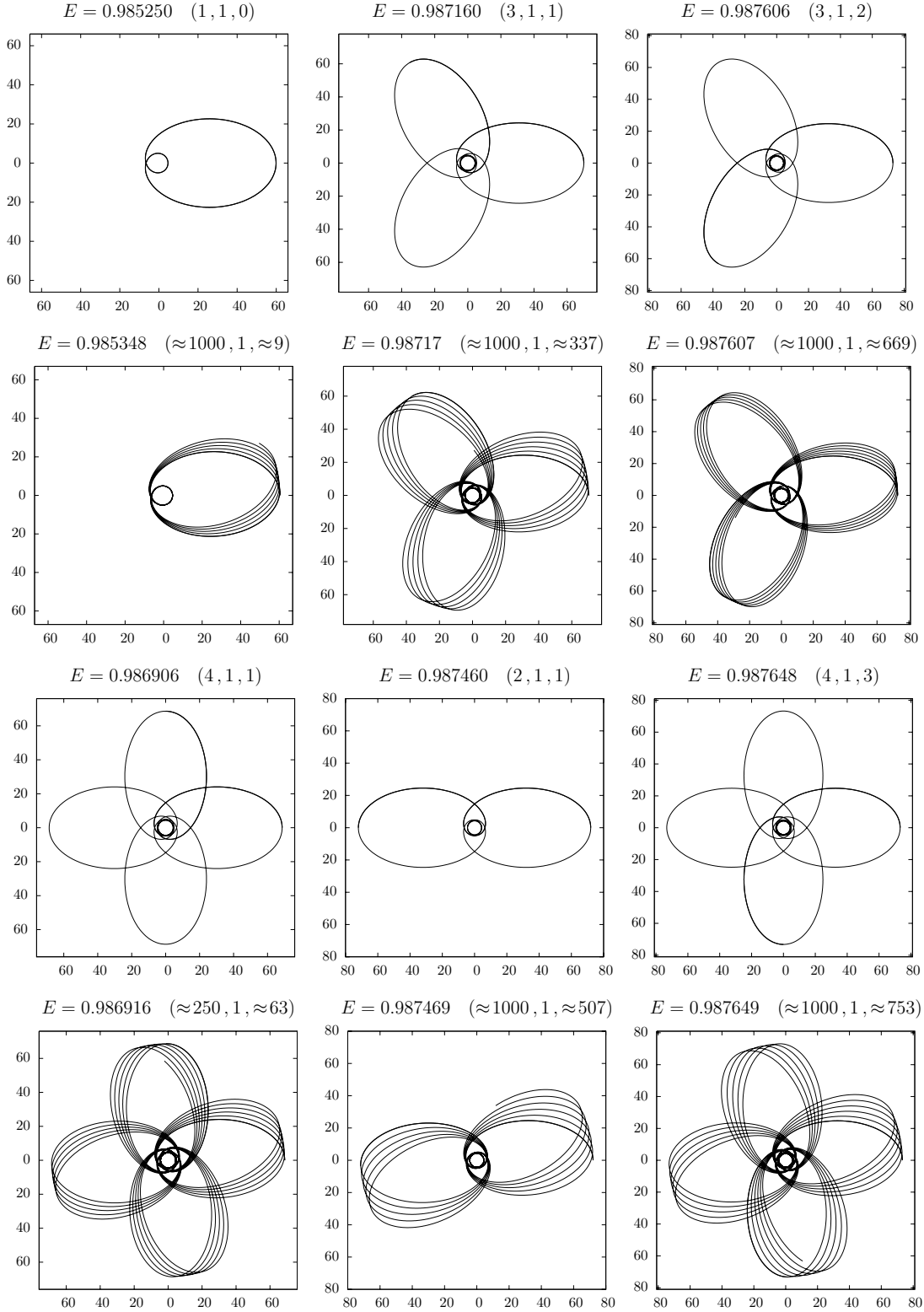


FIG. 12: A series of $w = 1$ orbits for the $L = 3.9$ line of figure 9. Orbits increase in energy from top to bottom and left to right. All $z = 1, 2, 3, 4$ orbits are shown. Also shown are randomly selected high z orbits. Notice that the high z orbits look like precessions of the energetically closest low z

entry in the sequence of periodic orbits is blank to indicate the complete absence of the $(1, 0, 0)$ orbit as discussed above. The second entry in the sequence is also blank indicating the complete absence of the $(3, 0, 1)$ orbit – as figure 9 shows, q never drops to $1/3$.

Figure 12, which was previewed in the introduction, shows the progression through orbits with higher numbers of zooms. All orbits are drawn from the $w = 1$ band – the middle column of figure 11. As before they are arranged in order of increasing energy from top to bottom and left to right. All orbits with $z = 1, 2, 3, 4$ are drawn. Between each of these low leaf orbits, randomly selected high zoom orbits are shown as well. The high zoom orbits look like precessions of the low zoom orbits.

Notice that for Schwarzschild the vast majority of low leaf orbits are stacked at high eccentricity. Orbits around spinning black holes, by contrast, show a wider spread of low z orbits at low eccentricities as we now demonstrate.

B. The Kerr zoo

Kerr orbits do not admit a simple one-dimensional effective potential description.⁶ Despite this complication, the generic Kerr system (appendix §A) has all the key features we need for our taxonomy. For any L , there is always one stable circular orbit. At some critical L a first bound unstable circular orbit will appear bringing with it an associated homoclinic orbit. The unstable circular orbit always has energy higher than that of the stable circular orbit. For a given $L_{ISCO} < L < L_{IBCO}$, the energy continues to specify uniquely orbits ranging from the stable circular to the homoclinic. Therefore, the same graphical analysis that we used to determine the population of the Schwarzschild zoo can be used to determine the population of the Kerr zoo.

Because the weak-field regimes look essentially the same for all a , we consider only values of $L_{ISCO} < L < L_{IBCO}$. As demonstrated for a Kerr black hole with spin $a = 0.995$ in figure 13(a), the rational numbers corresponding to closed orbits increase monotonically with energy. The rationals diverge at the homoclinic orbit for each L since the number of

⁶ There is an unappetizing effective potential description for equatorial orbits that we do not want to rely upon here.

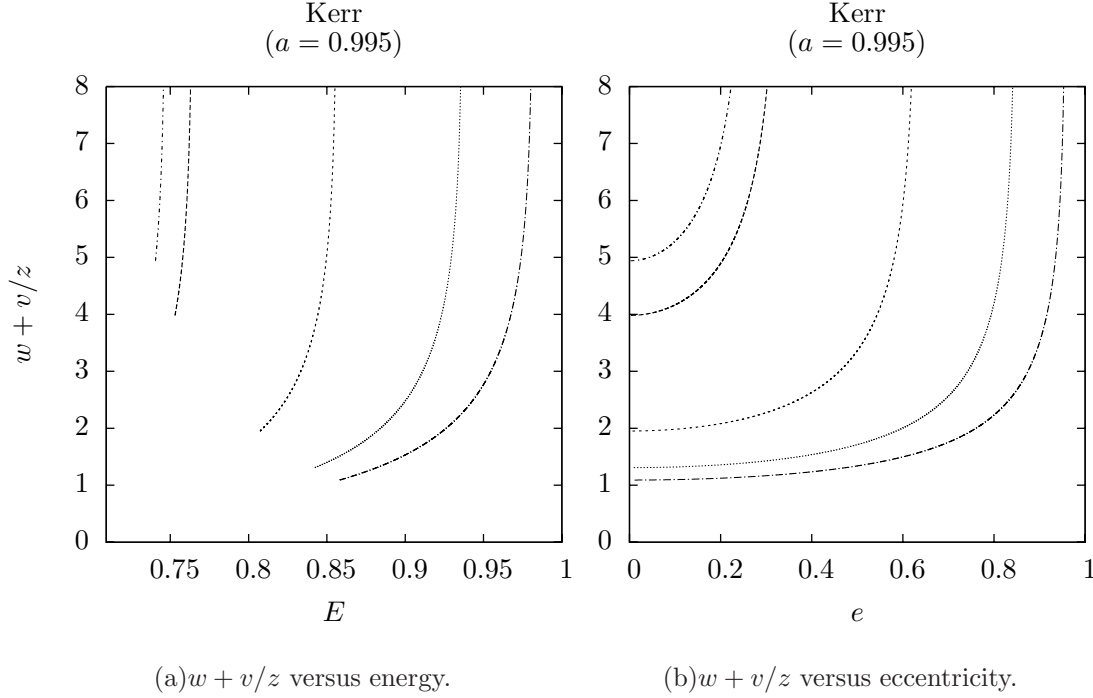


FIG. 13: Prograde orbits around a spinning black hole with $a = 0.995$. The lines indicate increasing L from left to right through the values $L = 1.57, 1.61, 1.82, 2, 2.1$

whirls diverges. The rationals are bounded from below by q_c at the stable circular orbit:

$$q_c \leq q \leq \infty \quad (19)$$

Figure 13(b). shows the increase of the rationals from the stable circular orbit to the homoclinic orbit is shown versus eccentricity for $a = 0.995$ and a range of L 's.

In contrast to the non-spinning case of figure 9, all eccentric orbits (with $L < L_{IBCO}$) have at least one whirl for such high spin. Generally, $a \neq 0$ orbits exhibit more whirls at low and intermediate eccentricities than their $a = 0$ counterparts. As eccentricity (and energy) increase for a given L , the number of whirls diverges as a homoclinic orbit is approached.

Figure 14 displays a periodic table, energy increasing from top to bottom through the $w = 3$ and $w = 4$ bands for $L = 1.82$. Each entry has a periodic orbit. All $z = 1, 2, 3, 4$ closed orbits are shown. The series shows the passage through these low leaf, moderate eccentricity orbits as energy – and therefore q increases.

Finally, figure 15 displays a periodic table with both low and high z orbits, energy increasing from top to bottom for $L = 2$ and $a = 0.995$. The sequence takes you through low leaf orbits to high leaf orbits that look very much like precessions of lower leaf periodics.

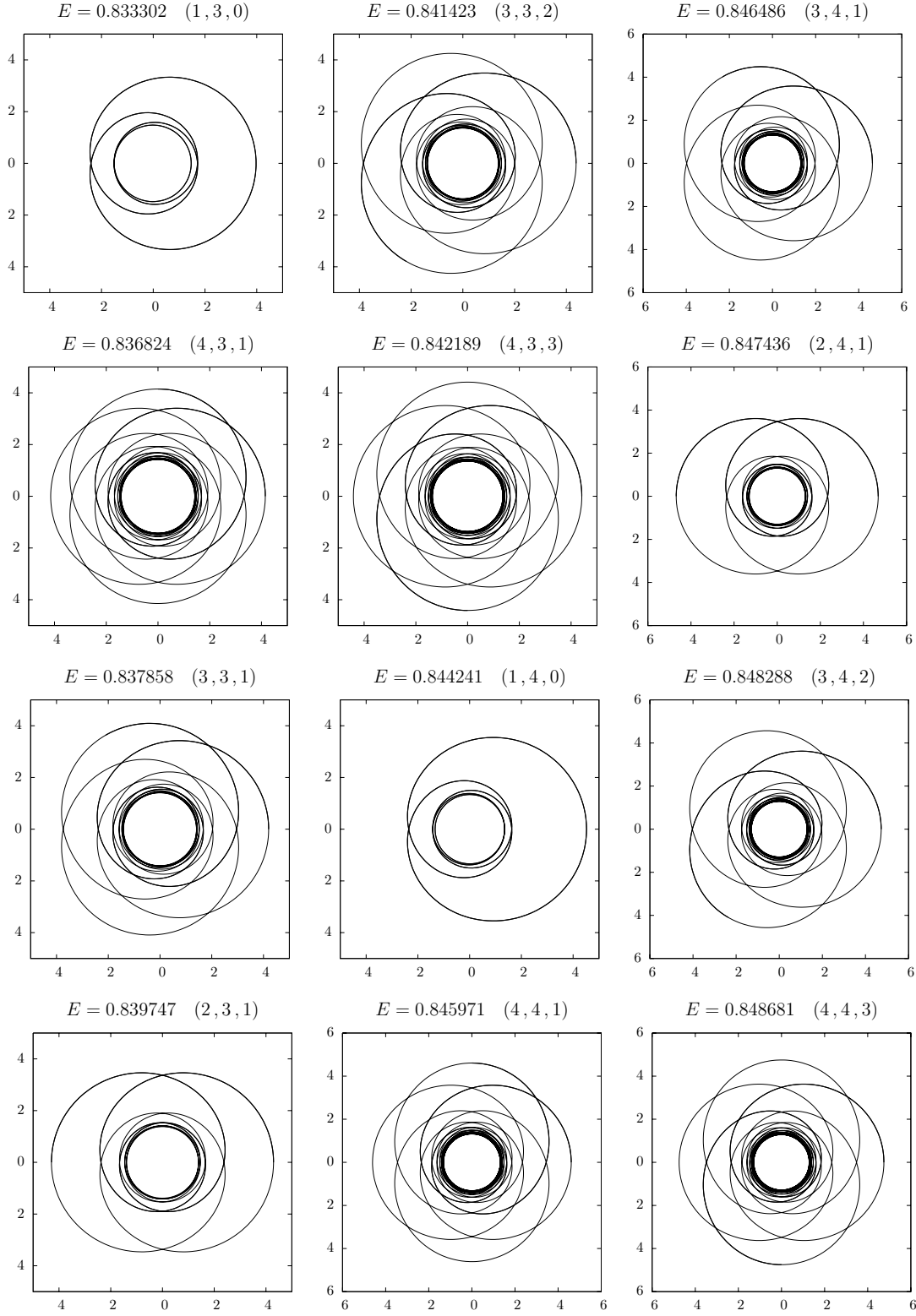


FIG. 14: A series of $w = 3$ and $w = 4$ orbits for the $L = 1.82$ line of figure 13. Orbits increase in energy from top to bottom and left to right. All $z = 1, 2, 3, 4$ orbits are shown.

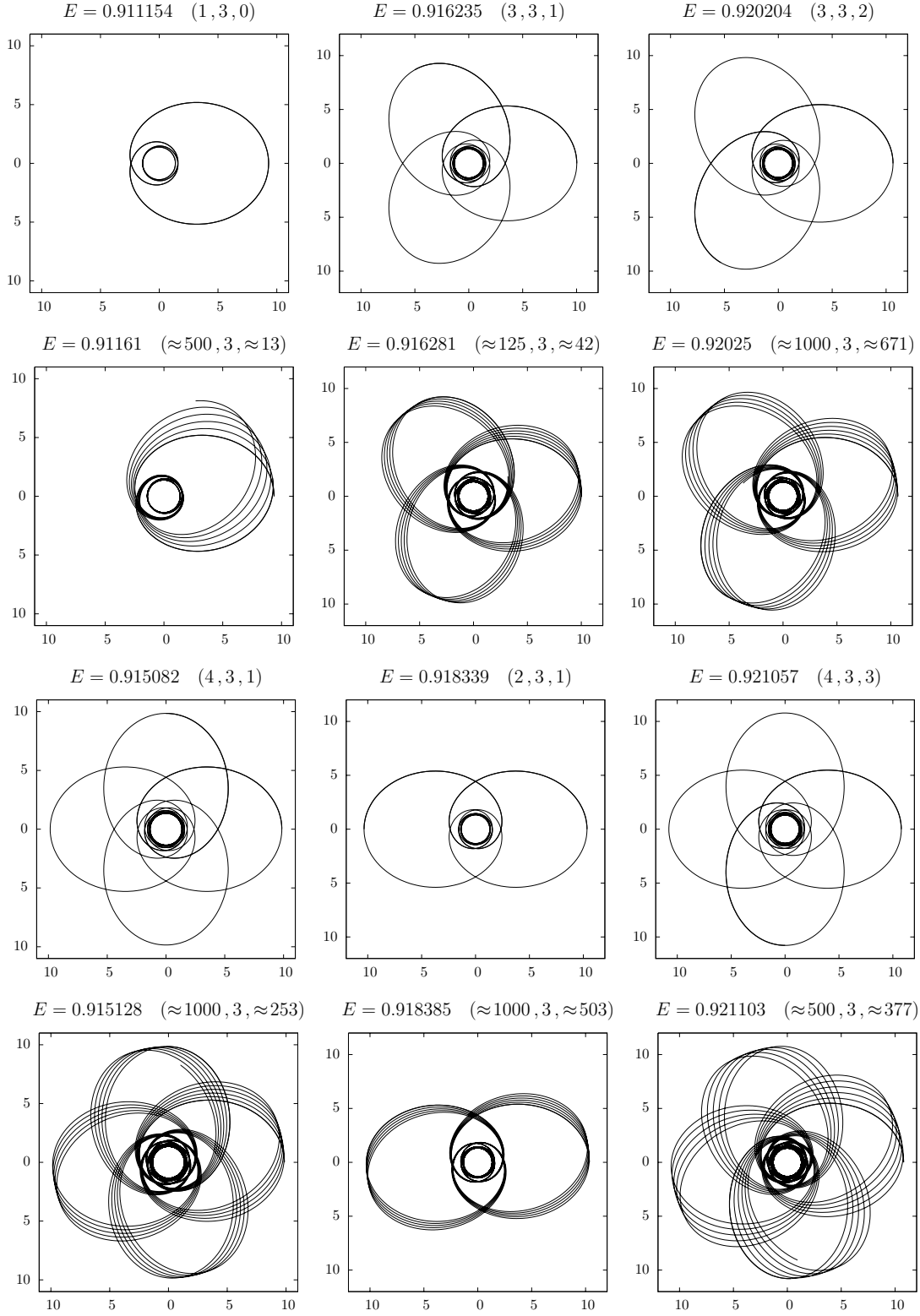


FIG. 15: A series of $w = 3$ orbits for the $L = 2$ line of figure 13. Orbits increase in energy from top to bottom and left to right. All $z = 1, 2, 3, 4$ orbits are shown. Also shown are randomly selected high z orbits. Notice that the high z orbits look like precessions of the energetically closest low z

The conclusion is that all eccentric Kerr orbits show zoom-whirl behavior of some kind for this a and $L < L_{IBCO}$. In the strong-field regime, once $L < L_{IBCO}$, the pattern of zoom-whirls at the lower energy bound looks like a precession of a low-leaf clover and at the upper energy bound marches toward homoclinic – a single leaf with an infinite number of whirls.

RECAP OF DYNAMICAL RESULTS

This concludes the primary results of the paper. Before turning to a discussion of astrophysical applications of the taxonomy, we briefly recap the results of this section:

- For a given a and L , all periodic orbits corresponding to rationals in the range

$$q_c \leq q \leq q_{max} \quad (20)$$

define the skeleton of the entire orbital dynamics, where q_c is the limiting rational associated with the stable circular orbit and q_{max} is the approximate rational of the maximum energy bound orbit.

- In the Newtonian limit, the upper and lower bounds both approach zero; Keplerian orbits are ellipses.
- There is no zoom-whirl behavior in the weak-field regime.
- At the ISCO, the upper and lower q bounds both approach ∞ because the ISCO is at once both a circular and a homoclinic orbit and all homoclinic orbits have $q = \infty$.
- In the very strong-field regime, which we take here to correspond to ($L < L_{IBCO}$), q has no upper bound:

$$q_c \leq q \leq \infty \quad (21)$$

- In the strong-field regime, the simple precessing ellipse familiar from planetary orbits is forbidden.
- *All* aperiodic eccentric orbits are precessions of low-leaf periodics.
- As the ISCO is approached, *all* orbits whirl as well as zoom for any a .

IV. APPLICATIONS AND FUTURE WORK

Our approach – representing the entire black hole dynamics in terms of a periodic skeleton – can be extended to non-equatorial orbits and then applied to astrophysical problems such

as gravitational wave astronomy and a dynamical analysis of spinning black hole pairs. We briefly describe each of these applications in turn.

Non-equatorial Orbits: Equatorial orbits yield especially well to a visual rendering of the properties of periodic orbits and their relationship to aperiodic ones. We focused here exclusively on equatorial orbits for precisely those pedagogic reasons. Already underway, our next order of business is to extend the periodic orbit analysis to non-equatorial Kerr geodesics. Generic non-equatorial trajectories can look complex particularly for high eccentricities and inclinations in the strong-field [18]. Still, periodic orbits must exist. Just as in the equatorial case periodic orbits will correspond to rational numbers. Identifying the ordering of those rationals with respect to those orbital parameters should offer an elegant and illuminating description of the dynamics.

Framing the non-equatorial periodic skeleton is not a solely academic enterprise. The modeling of extreme mass ratio inspirals (EMRIs) of compact objects into rotating supermassive black holes relies heavily on non-equatorial Kerr dynamics.

Gravitational Wave Astronomy: Compact objects orbiting supermassive black holes in galactic centers are expected to be plentiful sources for gravitational waves in the LISA bandwidth [15, 16]. Tens of thousands of such compact objects populate our own galactic center. Through gravitational scattering, a stellar mass compact object can be thrown into a highly eccentric orbit in the strong-field regime [26]. We have shown that all eccentric orbits show zoom behavior of some sort – that is to say, a pattern of discernible leaves – and large ranges of L and E generate whirl behavior (figures 9 and 13). In particular, in the strong-field regime, we should not expect eccentric orbits to be characterized by precessing ellipses, but rather by the precession of multi-leaf orbits. These EMRIs will therefore show the zoom-whirl behavior taxonomized in this paper.

So far we have only described the conservative dynamical system. Astrophysical objects orbiting near a massive black hole will radiate gravitational waves and veer off geodesics under the effects of dissipation. A study of adiabatic inspiral through periodic orbits might offer computational advantages. For instance, periodic orbits should have more rapidly converging Fourier series, than aperiodic ones. Additionally, the evolution of the conserved quantities E , L , and Q may not be independent, thereby cutting down dramatically on the computational expenses.

Closed orbits also show promise as a benefit to signal extraction from the gravitational

wave observatories in a time-frequency analysis. Furthermore, the templates of aperiodic orbits, where required [27], might be suitably replaced by periodic tables.

Spinning Pairs: The Kerr orbits are only integrable in the case of non-spinning test particles. If the companion spins, a constant of integration is lost (namely Q) and the dynamics is no longer integrable [28, 29]. While many of the other techniques for studying the dynamics may not generalize to spinning pairs, periodic orbits still define the skeleton of the phase space. Even if no clean taxonomy for those orbits exists, a search for and analysis of periodic orbits should reveal general properties of the dynamics.

Further, it is already known that spinning pairs can exhibit chaos [28, 29, 30, 31, 32, 33, 34, 35]. Treating spin of the companion as a perturbation to Kerr motion, the progression of closed orbits under that perturbation could track the transition to chaos. As the companion spin increases, the periodic orbits proliferate and the homoclinic orbit is replaced with a homoclinic tangle – a fractal set of unstable periodic orbits [12, 13]. A fractal in phase space of such rapidly spinning systems was revealed in Ref. [29] for comparable mass black hole binaries in the Post-Newtonian expansion by numerically scattering black holes. An analysis centered on periodic orbits should reveal the fractal set more readily, thereby removing the need to search and survey phase space blindly for chaotic behavior.

V. CONCLUSION

Periodic orbits structure the entire equatorial dynamics around black holes. In the spirit of Poincaré’s approach, we have defined a taxonomy of all periodic orbits based on zooms, whirls, and vertices and forged an explicit connection with the set of rational numbers. Under this scheme, all generic aperiodic orbits can always be approximated as near one of the periodics.

Our method reveals that no eccentric orbits will trace out planetary type elliptical precessions in the strong-field regime. Instead, all eccentric orbits are precessions of multi-leaf orbits with whirls multiplying as the black hole spins. The implication for gravitational wave astronomy is intriguing: all eccentric orbits will transition through these nearly periodic orbits as they inspiral to the plunge.

Acknowledgments

We are especially grateful to Becky Grossman for her valuable and generous contributions to this work and to Jamie Rollins for his careful reading of the manuscript, inspired suggestions, and for coining our figures “periodic tables”. We also thank Szabi Marka for valuable discussions of this work. JL and GP-G acknowledge financial support from a Columbia University ISE grant. This material is based in part upon work supported under a National Science Foundation Graduate Research Fellowship.

APPENDIX A: THE KERR EQUATIONS

We now present the explicit equations integrated to generate the results for §III A and IIIB. We will also derive the association between periodic orbits and rational numbers from the dynamical systems perspective. Since the natural language for that discussion is Hamiltonian mechanics, we begin with the Hamiltonian formulation of Kerr geodesic motion.

1. The Kerr Metric and Geodesic equations

In Boyer-Lindquist coordinates and geometrized units ($G = c = 1$), the Kerr metric is

$$ds^2 = -\mu^2 d\tau^2 = -\left(1 - \frac{2Mr}{\Sigma}\right) dt^2 - \frac{4Mar \sin^2 \theta}{\Sigma} dt d\varphi + \frac{\Sigma}{\Delta} dr^2 + \Sigma d\theta^2 + \sin^2 \theta \left(r^2 + a^2 + \frac{2Ma^2 r \sin^2 \theta}{\Sigma}\right) d\varphi^2 \quad . \quad (\text{A1})$$

Here

$$\begin{aligned} \Sigma &\equiv r^2 + a^2 \cos^2 \theta \\ \Delta &\equiv r^2 - 2Mr + a^2 \quad , \end{aligned} \quad (\text{A2})$$

and M, a denote the central black hole mass and spin angular momentum per unit mass, respectively. Besides the test particle mass μ , three additional quantities are conserved along Kerr geodesics: the energy E and z -component of angular momentum L as measured by observers at infinity, and the Carter constant Q . Following a useful and now common convention, we hereafter set both $M = 1$ and $\mu = 1$. This choice leaves the overall appearance of the metric and other Kerr expressions otherwise unchanged provided all Boyer-Lindquist coordinates, the proper time τ , the spin parameter a and all conserved quantities are now interpreted as dimensionless quantities.

Since they possess as many constants of motion (μ, E, L, Q) as degrees of freedom (t, r, θ, φ), the usually second order geodesic equations can be integrated to yield a set of 4 first order equations of motion for the coordinates [4],

$$\begin{aligned} \Sigma \dot{r} &= \pm \sqrt{R} \\ \Sigma \dot{\theta} &= \pm \sqrt{\Theta} \\ \Sigma \dot{\varphi} &= -\left(aE - \frac{L}{\sin^2 \theta}\right) + \frac{a}{\Delta} P \end{aligned}$$

$$\Sigma \dot{t} = -a (aE \sin^2 \theta - L) + \frac{r^2 + a^2}{\Delta} P \quad , \quad (\text{A3})$$

where an overdot denotes differentiation with respect to the particle's proper time τ and

$$\begin{aligned} \Theta(\theta) &= Q - \cos^2 \theta \left\{ a^2(1 - E^2) + \frac{L^2}{\sin^2 \theta} \right\} \\ P(r) &= E(r^2 + a^2) - aL \\ R(r) &= P^2 - \Delta \{ r^2 + (L - aE)^2 + Q \} \quad . \end{aligned} \quad (\text{A4})$$

We note that while these equations are concise and appealing in some ways, during numerical integration they tend to accumulate error at the turning points due to the explicit square roots in the r and θ equations, not to mention the nuisance of having to change the signs of the r and θ velocities by hand at every turning point. While other authors circumvent this problem with a rather involved reparametrization of the equations in (A3), we will see that in a Hamiltonian formulation the numerical difficulties are avoided naturally.

2. Hamiltonian Formulation of Kerr Geodesic Motion

We begin with a Lagrangian for a free particle in the Kerr spacetime:

$$\mathcal{L} = \frac{1}{2} g_{\alpha\beta} \dot{q}^\alpha \dot{q}^\beta \quad . \quad (\text{A5})$$

Because the q^α are dimensionless coordinates ($\mu = 1$), and because $g_{\alpha\beta} \dot{q}^\alpha \dot{q}^\beta = -1$ for timelike trajectories, eqn. (A1) implies that \mathcal{L} is identically equal to $-1/2$ along any trajectory. The particle's 4-momentum

$$p^\alpha \equiv \dot{q}^\alpha$$

is also dimensionless and is identical to the 4-velocity. Defining the canonical momentum p_α for the system in the standard way, we see that it coincides with the 4-momentum one-form,

$$p_\alpha \equiv \frac{\partial \mathcal{L}}{\partial \dot{q}^\alpha} \quad (\text{A6})$$

$$= g_{\alpha\beta} \dot{q}^\beta = g_{\alpha\beta} p^\beta \quad . \quad (\text{A7})$$

Explicitly, the components of the momentum⁷ are

$$p_t = - \left(1 - \frac{2r}{\Sigma} \right) \dot{t} - \frac{2ar \sin^2 \theta}{\Sigma} \dot{\varphi} \quad (\text{A8})$$

⁷ “Momentum” will always refer to the canonical momentum, i.e. the momentum one-form on the spacetime, unless otherwise noted.

$$p_r = \frac{\Sigma}{\Delta} \dot{r} \quad (\text{A9})$$

$$p_\theta = \Sigma \dot{\theta} \quad (\text{A10})$$

$$p_\varphi = \sin^2 \theta \left(r^2 + a^2 + \frac{2a^2 r \sin^2 \theta}{\Sigma} \right) \dot{\varphi} \quad (\text{A11})$$

$$- \frac{2ar \sin^2 \theta}{\Sigma} \dot{t} \quad . \quad (\text{A12})$$

We finally define the Hamiltonian in the standard way,

$$H = p_\mu \dot{q}^\mu - \mathcal{L} = \frac{1}{2} g^{\alpha\beta} p_\alpha p_\beta \quad . \quad (\text{A13})$$

Note that the Hamiltonian is numerically identical to our Lagrangian ($-1/2$) along any orbit because each quantity is just half the contraction of the 4-momentum. This is not surprising since, for geodesic motion, the Lagrangian and Hamiltonian contain only kinetic terms.

To get an explicit expression for the Hamiltonian in terms of our dimensionless coordinates and momenta, we could compute the inverse metric $g^{\alpha\beta}$ and grind through eqn. (A13) by brute force. However, a simple observation yields a nice expression for $H(q, p)$ with much less effort. Using eqns. (A9)-(A10) in eqn. (A5), we know the Hamiltonian must have the form

$$H(\mathbf{q}, \mathbf{p}) = \frac{\Delta}{2\Sigma} p_r^2 + \frac{1}{2\Sigma} p_\theta^2 + f(r, \theta, p_t, p_\varphi) \quad , \quad (\text{A14})$$

where f is a function yet to be determined that depends only on p_t and p_φ and, via the $g^{\alpha\beta}$, on r and θ . Eliminating the p_r and p_θ above with the use of (A8) and (A3) and noting that H must identically equal $-1/2$, we see that

$$H(\mathbf{q}, \mathbf{p}) = \frac{R}{2\Delta\Sigma} + \frac{\Theta}{2\Sigma} + f(r, \theta, p_t, p_\varphi) = -1/2 \quad . \quad (\text{A15})$$

This fixes f and allows us finally to write H as

$$H(\mathbf{q}, \mathbf{p}) = \frac{\Delta}{2\Sigma} p_r^2 + \frac{1}{2\Sigma} p_\theta^2 - \frac{R + \Delta\Theta}{2\Delta\Sigma} - \frac{1}{2} \quad , \quad (\text{A16})$$

where R and Θ are the functions listed in eqns. (A4) with every E or L therein interpreted as a $-p_t$ or p_φ , respectively, and with every Q treated as a constant.

With the Hamiltonian written as in (A16), Hamilton's equations

$$\dot{q}_i = \frac{\partial H}{\partial p_i} \quad , \quad \dot{p}_i = -\frac{\partial H}{\partial q_i} \quad (\text{A17})$$

for the test particle motion become, explicitly,

$$\dot{r} = \frac{\Delta}{\Sigma} p_r \quad (\text{A18})$$

$$\begin{aligned} \dot{p}_r &= - \left(\frac{\Delta}{2\Sigma} \right)' p_r^2 - \left(\frac{1}{2\Sigma} \right)' p_\theta^2 + \left(\frac{R + \Delta\Theta}{2\Delta\Sigma} \right)' \\ \dot{\theta} &= \frac{1}{\Sigma} p_\theta \\ \dot{p}_\theta &= - \left(\frac{\Delta}{2\Sigma} \right)^\theta p_r^2 - \left(\frac{1}{2\Sigma} \right)^\theta p_\theta^2 + \left(\frac{R + \Delta\Theta}{2\Delta\Sigma} \right)^\theta \\ \dot{t} &= \frac{1}{2\Delta\Sigma} \frac{\partial}{\partial E} (R + \Delta\Theta) \end{aligned} \quad (\text{A19})$$

$$\begin{aligned} \dot{p}_t &= 0 \\ \dot{\varphi} &= - \frac{1}{2\Delta\Sigma} \frac{\partial}{\partial L} (R + \Delta\Theta) \\ \dot{p}_\varphi &= 0, \end{aligned} \quad (\text{A20})$$

where the superscripts $'$ and θ denote differentiation with respect to r and θ , respectively. Note that since none of the equations contain square roots any more, they constitute a smoothly differentiable system of ODEs, even at turning points, and they can be integrated directly without resorting to an intricate change of variable. Since the \dot{p}_t and \dot{p}_φ equations vanish, the only added cost of retaining analytical transparency in the equations is that we must integrate 6 equations in (A18) instead of 4 in (A3). These are the equations we integrate numerically to identify the periodic orbits.

We isolate the periodic orbits by inputting (z, w, v) for a given a and L to locate the E , apastron r_a and perihelion r_p of the corresponding periodic orbit. Numerically the periodics are extracted by explicitly integrating

$$\Delta\varphi_r = 2 \int_{t(r_p)}^{t(r_a)} \frac{d\varphi}{dt} dt = 2 \int_{r_p}^{r_a} \frac{d\varphi}{dr} dr \quad (\text{A21})$$

to find those orbits for which the integral is a rational multiple of 2π .

As a final check of our numerical results, we run an independent code that computes the orbits directly from the geodesic equation and find the two independent computations in complete accord.

APPENDIX B: THE ACTION-ANGLE PICTURE

In addition to deriving numerically solve equations of motion, we can use Hamiltonian dynamics to relate the periodic orbits to rationally related canonical frequencies. We now relate those frequencies to the taxonomy we have developed.

It is a classic result of Hamiltonian dynamics that motion in a system with N coordinates and N conserved momenta will be confined to N -dimensional tori. In this case we do have 4 coordinates (t, r, θ, φ) and 4 conserved quantities (μ, E, L, Q) . However, this classic result only applies to orbits bound in phase space. In our relativistic system, the t direction throws a wrench in the works since every orbit increases without bound in the timelike direction – worldlines, in both phase space and configuration space, are not compact. To circumvent this problem, we work in a formally *reduced phase space*.⁸ Any canonical coordinate can be chosen as the time parameter and its canonical momentum will become the Hamiltonian for the reduced phase space [22]. In our case, we choose to parameterize the orbits by t and use $p_t = E$ as the Hamiltonian of the reduced phase space.

In this paper we are only dealing with equatorial motion, for which motion lies in the 4D hypersurface defined by $\theta \equiv \pi/2, p_\theta \equiv 0$ and on which $Q \equiv 0$. On that hypersurface r, φ, p_r and p_φ still form a canonical set, so the hypersurface corresponding to equatorial orbits constitutes a *bona fide* 4D phase space.

On this space, all phase space trajectories corresponding to orbits that are bound and non-plunging in configuration space lie on compact hypersurfaces topologically equivalent to 2D tori. Thus, we can make the transformation to action-angle variables for those orbits, to which we now turn.

A canonical transformation to action variables allows us to set each canonical momentum J_i equal to a function of the constants of motion. The reduced Hamiltonian can be rewritten as a function of the \mathbf{J} only,

$$E = E(\mathbf{J}) \quad , \quad (\text{B1})$$

so that it is cyclic in all the ψ_i , and the (ψ_i, J_i) form a canonical set whose evolution is still determined by Hamilton's equations

$$\frac{dJ_i}{dt} = -\frac{\partial E}{\partial \psi_i}$$

⁸ A more detailed exposition of which we leave to the nonequatorial case.

$$\frac{d\psi_i}{dt} = \frac{\partial E}{\partial J_i} \quad , \quad (\text{B2})$$

($i = r, \varphi$). Together, (B1) and (B2) imply that each J_i is a constant of the motion and that each ψ_i is linear in time,

$$\psi_i = \omega_i t + \psi_i(0) \quad , \quad (\text{B3})$$

where each

$$\omega_i(\mathbf{J}) \equiv \dot{\psi}_i = \frac{\partial E(\mathbf{J})}{\partial J_i} \quad (\text{B4})$$

is a function only of the J_i and thus also a constant of the motion. These constants are the orbital frequencies used as a basis in which to Fourier decompose functions of generic Kerr orbits, including the instantaneous adiabatic gravitational waveforms they emit [23, 24].

We define the radial and azimuthal actions in the standard way, as

$$J_r = \frac{1}{2\pi} \oint_{C_r} p_r dr \quad (\text{B5})$$

$$J_\varphi = \frac{1}{2\pi} \oint_{C_\varphi} p_\varphi d\varphi \quad , \quad (\text{B6})$$

where the curves C_r and C_φ are projections of the orbit into the $r - p_r$ and $\varphi - p_\varphi$ planes, respectively. Because p_φ is a constant we see that

$$J_\varphi \equiv p_\varphi = L \quad . \quad (\text{B7})$$

We are more interested in the frequencies ω_r and ω_φ . An explicit expression for the Hamiltonian in terms of the J 's requires inverting the J_r integral in (B5) to solve for $E(J_r, L) = E(J_r, J_\varphi)$ and thus is not analytically accessible. Still, expressions for the ω_i in terms of E, L rather than in terms of J_r, J_φ *can* be computed as follows.

Since a trajectory can alternately be specified by constants of the motion (E, L) or (J_r, J_φ) , there exists some transformation from the (E, L) set to the J_r, J_φ set. Since

$$J_\varphi(E, L) \equiv L \quad , \quad (\text{B8})$$

the Jacobian of the transformation is

$$\begin{vmatrix} \frac{\partial J_r}{\partial E} & \frac{\partial J_r}{\partial L} \\ \frac{\partial J_\varphi}{\partial E} & \frac{\partial J_\varphi}{\partial L} \end{vmatrix} = \begin{vmatrix} \frac{\partial J_r}{\partial E} & \frac{\partial J_r}{\partial L} \\ 0 & 1 \end{vmatrix} = \frac{\partial J_r}{\partial E} \quad , \quad (\text{B9})$$

which, since J_r increases monotonically with E at a given L , never vanishes. There thus exists an inverse transformation $E(J_r, J_\varphi), L(J_r, J_\varphi)$ from the actions back to the usual orbital constants. The product of those two transformations should be identity:

$$\begin{pmatrix} \frac{\partial J_r}{\partial E} & \frac{\partial J_r}{\partial L} \\ \frac{\partial J_\varphi}{\partial E} & \frac{\partial J_\varphi}{\partial L} \end{pmatrix} \begin{pmatrix} \frac{\partial E}{\partial J_r} & \frac{\partial E}{\partial J_\varphi} \\ \frac{\partial L}{\partial J_r} & \frac{\partial L}{\partial J_\varphi} \end{pmatrix} = \begin{pmatrix} \frac{\partial J_r}{\partial E} & \frac{\partial J_r}{\partial L} \\ 0 & 1 \end{pmatrix} \begin{pmatrix} \frac{\partial E}{\partial J_r} & \frac{\partial E}{\partial J_\varphi} \\ 0 & 1 \end{pmatrix} = \begin{pmatrix} 1 & 0 \\ 0 & 1 \end{pmatrix} \quad , \quad (\text{B10})$$

which is equivalent to the two independent equations

$$\frac{\partial J_r}{\partial E} \frac{\partial E}{\partial J_r} = 1 \quad (\text{B11})$$

$$\frac{\partial J_r}{\partial E} \frac{\partial E}{\partial J_\varphi} = -\frac{\partial J_r}{\partial L} \quad . \quad (\text{B12})$$

But in our reduced phase space, E is the reduced Hamiltonian, so each $\partial E / \partial J_i \equiv \omega_i$. The equations above then yield

$$\begin{aligned} \omega_r &= \frac{1}{\partial J_r / \partial E} \\ \omega_\varphi &= -\frac{\partial J_r / \partial L}{\partial J_r / \partial E} \quad . \end{aligned} \quad (\text{B13})$$

Combining equations (A8), (A4) and (B5), we see that

$$\oint_{C_r} p_r dr = 2 \int_{r_p}^{r_a} dr \frac{\sqrt{R}}{\Delta} \quad (\text{B14})$$

and, combining this with the equations of motion, that

$$\begin{aligned} -\frac{\partial J_r}{\partial L} &= -\frac{1}{2\pi} 2 \frac{\partial}{\partial L} \int_{r_p}^{r_a} dr \frac{\sqrt{R}}{\Delta} \\ &= \frac{1}{2\pi} 2 \int_{r_p}^{r_a} dr \frac{1}{2\sqrt{R}\Delta} \left(-\frac{\partial R}{\partial L} \right) \end{aligned}$$

where the term proportional to the partial of the limits vanishes since the integrand vanishes at the limits. Continuing,

$$\begin{aligned} -\frac{\partial J_r}{\partial L} &= \frac{1}{2\pi} 2 \int_{r_p}^{r_a} dr \frac{\Sigma}{\sqrt{R}} \frac{-\partial R / \partial L}{2\Delta\Sigma} \\ &= \frac{1}{2\pi} 2 \int_{r_p}^{r_a} dr \frac{\dot{\varphi}}{\dot{r}} \\ &= \frac{1}{2\pi} \Delta\varphi_r \quad , \end{aligned} \quad (\text{B15})$$

where the last equality comes from equation (7). Additionally,

$$\begin{aligned}
\frac{\partial J_r}{\partial E} &= \frac{1}{2\pi} 2 \frac{\partial}{\partial E} \int_{r_p}^{r_a} dr \frac{\sqrt{R}}{\Delta} \\
&= \frac{1}{2\pi} 2 \int_{r_p}^{r_a} dr \frac{1}{2\sqrt{R}\Delta} \left(\frac{\partial R}{\partial E} \right) \\
&= \frac{1}{2\pi} 2 \int_{r_p}^{r_a} dr \frac{\Sigma}{\sqrt{R}} \frac{\partial R / \partial E}{2\Delta\Sigma} \\
&= \frac{1}{2\pi} 2 \int_{r_p}^{r_a} dr \frac{\dot{t}}{\dot{r}} \\
&= \frac{1}{2\pi} T_r \quad ,
\end{aligned} \tag{B16}$$

where T_r is the radial period of an orbit.

The physical interpretation of the ω 's is now clear. As expected, ω_r is

$$\omega_r = \frac{2\pi}{\int_{r_p}^{r_a} dr \frac{1}{\Delta\sqrt{R}}} \frac{\partial R}{\partial E} = \frac{2\pi}{T_r} \quad , \tag{B17}$$

where T_r as measured in coordinate time t . The rate at which azimuth accumulates averaged over the radial period is ω_φ :

$$\omega_\varphi = \frac{-\int_{r_p}^{r_a} dr \frac{1}{\Delta\sqrt{R}} \frac{\partial R}{\partial L}}{\int_{r_p}^{r_a} dr \frac{1}{\Delta\sqrt{R}} \frac{\partial R}{\partial E}} = \frac{\Delta\varphi_r}{T_r} \quad . \tag{B18}$$

Because for a periodic orbit, the total orbital period is an integer multiple of T_r (in fact, zT_r), we can equivalently say that ω_φ is the rate of increase of φ averaged over the entire orbital period (this latter interpretation is what will generalize when we leave the equatorial plane).

Finally, to make the connection with the §II B, note that the frequency ratio

$$\frac{\omega_\varphi}{\omega_r} = \frac{\Delta\varphi_r}{2\pi} = 1 + w + \frac{v}{z} = 1 + q \quad . \tag{B19}$$

Thus, in the action-angle picture, the periodic orbits are those with rationally related fundamental frequencies.

A typical orbit will fill out the torus because the canonical angular frequencies are not commensurate. In contrast, closed orbits do not. It is precisely this relation we have exploited to explicitly locate the periodic orbits in our taxonomy.

APPENDIX C: CIRCULAR ORBITS REVISITED

As discussed briefly in §II C, circular orbits, while clearly periodic, are somewhat anomalous in the geometric picture and our (z, w, v) scheme. After all, our taxonomy hinges on quantities calculated per radial period. Since the radial period of a circular orbit is zero, it is not clear what rational number to associate with circular orbits. Nevertheless, it turns out that in a useful and enlightening sense, some stable circular orbits (a measure zero set of them, to be precise) *are* mappable to the rational numbers. Naively, we might expect them to correspond to the rational number 1, just like Keplerian circular orbits, but this turns out to be a mistake.

The action-angle picture is significantly more informative here. Our difficulty stems from the fact that all circular orbits have a vanishing radial action J_r . In a loose sense, the actions correspond to the two circumferences that characterize a two-dimensional torus. When one of those circumferences is zero, the 2-torus T^2 just becomes a 1-torus $T^1 \equiv S^1$: a circle. Orbits that are circular in configuration space thus live on surfaces in the phase space that also have the topology of circles. In that sense, circular orbits only really have one fundamental frequency, ω_φ , and there is no rational frequency ratio to speak of. They are all nonetheless periodic, for any value of ω_φ , because any curve that fills out S^1 with a constant velocity necessarily closes on itself and becomes periodic.⁹

Nonetheless some stable circular orbits can be mapped to the rational numbers. We can construct that map in two equivalent ways. First, for a given L , we can take the zero eccentricity limit of the values of ω_r, ω_φ , and their ratio and define the corresponding values for the circular orbit with that same L to be those limits. This was the attitude taken in §II C.

Alternately, we can perform a linear stability analysis of the circular orbits. We find the frequencies of small oscillations of the r and φ motions of low eccentricity orbits around the r

⁹ Note that for spherical orbits, i.e. constant r orbits not confined to the equatorial plane, which other authors usually refer to as “non-equatorial circular orbits”, this will no longer be the case. Non-equatorial orbits in general have 3 associated actions J_r, J_θ and J_φ and are confined to surfaces with the topology of T^3 . On spherical orbits, J_r vanishes, but the remaining actions do not, leaving spherical orbits to occupy surfaces with the topology of T^2 . Much like generic equatorial orbits, then, spherical orbits will only be exactly periodic only when the ratio of their frequencies $\omega_\theta/\omega_\varphi$ is rational.

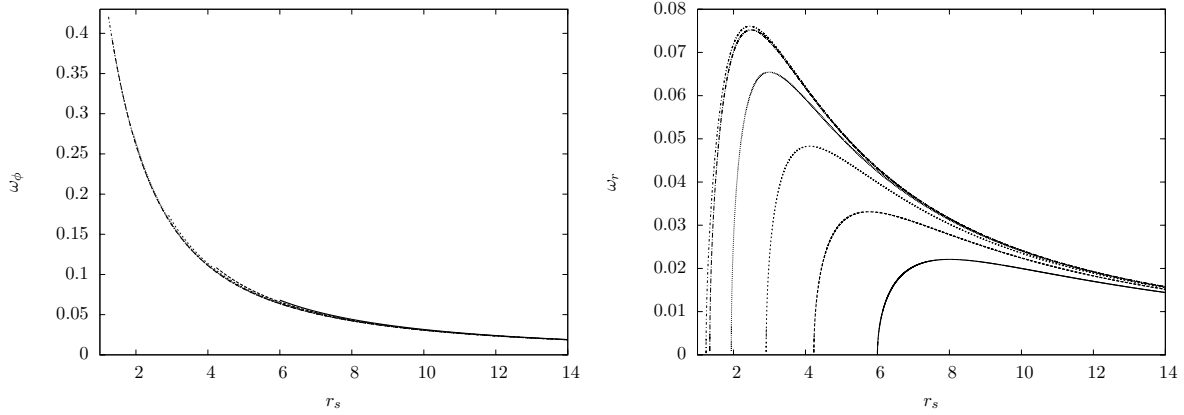


FIG. 16: Left: ω_ϕ versus the radii of stable circular orbits. Right: ω_r versus the radii of stable circular orbits. Increasing from right to left the spin values are $a = 0, 0.5, 0.8, 0.95, 0.995, 0.998$. All orbits are prograde.

and φ motions of the reference circular orbits and examine the ratios of those frequencies¹⁰.

Whether derived from a stability analysis or as the limiting values of low eccentricity orbits, figure 16 shows the resulting values of ω_ϕ and ω_r while figure 17 shows ω_ϕ/ω_r for stable circular orbits as a function of their radial coordinate r for various values of a . Some features are worth noting. First, ω_ϕ for a circular orbit is just the coordinate angular velocity and thus satisfies

$$\omega_\phi = \frac{d\phi}{dt} = \pm \frac{1}{r^{3/2} \pm a} \quad , \quad (\text{C1})$$

the well-known relativistic generalization of Kepler's third law [25]. Second, the ω_r 's differ from the Keplerian in that the increase with decreasing r until they hit some maximum (in the Keplerian case, the ω_r continue to increase and diverge at $r = 0$), at which point they decrease, reaching zero at the ISCO. The ISCO, then, will have a diverging ω_ϕ/ω_r ratio, an observation that was relevant in our discussion of homoclinic orbits. All homoclinic orbits have $q = w + v/z = \omega_\phi/\omega_r = \infty$, including the ISCO is (the eccentricity zero homoclinic orbit).

Third, ω_ϕ/ω_r for circular orbits is a continuous and monotonic function of r , increasing from an asymptotic value of 1 in the $r \rightarrow \infty$ limit and diverging as $r \rightarrow r_{ISCO}$. The continuity of this ratio means that although a measure zero subset of the circular orbits corresponds to rational numbers or, equivalently, to (z, w, v) triplets, most do not. Nevertheless, even

¹⁰ Often called epicycle frequencies, or just epicycles for short

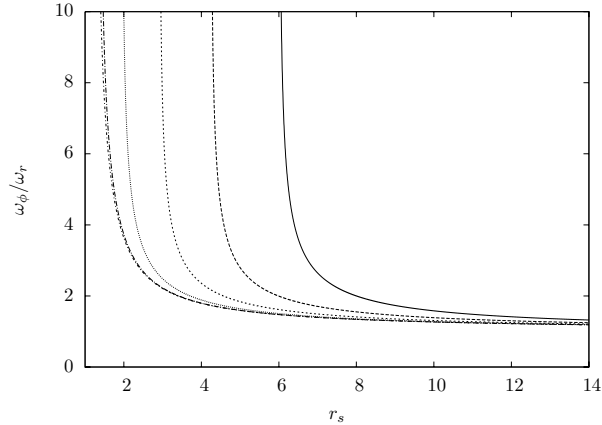


FIG. 17: The ratio ω_ϕ/ω_r , which equals $1 + w + v/z$, as a function of the radii of stable circular orbits. Increasing from right to left the spin values are $a = 0, 0.5, 0.8, 0.95, 0.995, 0.998$. All orbits are prograde.

the irrational circulars are arbitrarily close to some rational. We can thus characterize every circular orbit either exactly (the rational circulars) or approximately (the irrational circulars) by a (z, w, v) triplet.

Finally, dissipative dynamical systems with multiple coupled frequencies, can sometimes attractors (or at least transient attractors). Those attractors typically correspond to rationals q with low denominator fractional parts (low z). The 1 : 1 and 3 : 2 spin-orbit frequency ratios of the moon-earth and Mercury-sun systems, respectively, are solar system examples of where this sort of behavior takes place. The possibility that an orbit decaying adiabatically under radiation reaction might become trapped in a resonance en route to plunge is thus open. At the time of submission of this article, we are still investigating that possibility.

-
- [1] A. Fölsing, *Albert Einstein* (Viking Penguin: New York, 1997)
 - [2] L. Barack and C. Cutler, Phys. Rev. D **69**, 082005 (2004)
 - [3] K. Glampedakis and D. Kennefick, Phys. Rev. D **66**, 044002 (2002) (gr-qc/0203086)
 - [4] B. Carter, Phys. Rev. **174**, 1559 (1968)
 - [5] S. Chandrasekhar, *The Mathematical Theory of Black Holes* (Oxford: Clarendon Press, 1983)
 - [6] H. Poincaré, *Méthodes Nouvelles de la Mécanique Céleste* (Gauthier Villars: Paris, 1892)
 - [7] S. Chandrasekhar, Proc. R. Soc. Lond. **A421**, 227 (1989)

- [8] G. Contopoulos, in *Deterministic Chaos in General Relativity* ed. D. Hobill, A. Burd, and A. Coley (Plenum Press: New York, 1993) p.120
- [9] G. Contopoulos, Proc. R. Soc. Lond. **A431**, 183 (1990)
- [10] G. Contopoulos, Proc. R. Soc. Lond. **A435**, 551 (1991)
- [11] R. Moeckel, Commun. Math. Phys. **150**, 415 (1992)
- [12] C.P. Dettmann, N. E. Frankel & N.J. Cornish, Phys. Rev. D **50**, R618 (1994); Ibid, Fractals, **3**, 161 (1995).
- [13] L. Bombelli and E. Calzetta, Class. and Quant. Grav. **9**, 2573 (1992)
- [14] R. Wald, *General Relativity* (Chicago, 1984)
- [15] C. Hopman, AIP Conf.Proc.873 (2006) p.241(astro-ph/0608460)
- [16] S. Hughes, AIP Conf.Proc.873 (2006) p.233 (gr-qc/0608140)
- [17] J. E. McClintock, R. Shafee, R. Narayan, R. A. Remillard, S. W. Davis, L-X. Li, Astrophys.J.652, 518-539 (2006) (astro-ph/0606076)
- [18] S. Drasco and S. Hughes, Phys. Rev. D **73** 024027 (2006) (gr-qc/0509101)
- [19] S. Drasco, E. Flanagan, and S. Hughes, Class. and Quant. Grav. **22** S801 (2005) (gr-qc/0505075)
- [20] J. Levin, R. O'Reilly, and E. J. Copeland, Phys. Rev. D **62**, 024023 (2000) (gr-qc/9909051)
- [21] G. Perez-Giz, B. Grossman, and J. Levin, in preparation.
- [22] E. T. Whittaker, *Analytical Dynamics* (Cambridge University Press: Cambridge, 1961)
- [23] W. Schmidt, Class. Quant. Grav. **19**, 2743 (2002)
- [24] S. Drasco and S. A. Hughes, Phys. Rev. D **69**, 044015 (2004)
- [25] J. Bardeen, W. Press, and S. Teukolsky, Astrophys. J. **178**, 347 (1972)
- [26] P. Amaro-Seoane, J. R. Gair, M. Freitag, M. Coleman Miller, I. Mandel, C. J. Cutler, and S. Babak, Class. Quant. Grav. **24**, R113-R170 (2007) (astro-ph/0703495)
- [27] E. Poisson, Living Rev.Rel.7:6 (2004) (gr-qc/0306052)
- [28] S. Suzuki & K. Maeda, Phys. Rev. D **55**, 4848 (1997) (gr-qc/9604020)
- [29] J. Levin, Phys. Rev. Lett. **84**, 3515 (2000) (gr-qc/9910040)
- [30] J. Levin, Phys. Rev. D **67**, 044013 (2003) (gr-qc/0010100)
- [31] N. J. Cornish and J. Levin, Phys. Rev. D **68**, 024004 (2003) (gr-qc/0207016)
- [32] M. Hartl and A. Buonanno, Phys. Rev. D **71**, 024027 (2005) (gr-qc/0407091)
- [33] J. Levin, Phys. Rev. D **74**, 124027 (2006) (gr-qc/0612003)

- [34] M. Hartl, Phys. Rev. D **67**, 024005 (2003) (gr-qc/0210042)
- [35] M. Hartl, Phys. Rev. D **67**, 104023 (2003) (gr-qc/0302103)